ARTICLE

Life and death of liquid-infused surfaces: a review on the choice, analysis and fate of the infused liquid layer

Received 00th January 20xx,
Accepted 00th January 20xx

DOI: 10.1039/x0xx00000x

Sam Peppou-Chapman,[a,b] Jun Ki Hong,[a,b,c,d,e] Anna Waterhouse[b,c,d,e] & Chiara Neto[a,b]*

Liquid-infused surfaces (or lubricant-infused surfaces) (LIS) are a new class of functional materials introduced in 2011. Their exceptional properties have earned them a place at the forefront of many fields including anti-biofouling, anti-icing, anti-corrosion, drag reduction, droplet manipulation and drop-wise condensation. Integral to their success is the infused lubricant layer which affords them their properties. In this review, we examine the current state of the literature relating to the lubricant layer. We consider the lubricant through all stages in the surface's lifecycle from design, to use, all the way through to depletion and eventual failure. First, we examine trends in lubricant choice and how to choose a lubricant, including environmental and medical considerations. We then look at the different methods used to infuse lubricant into surfaces and how lubricant depletes from the surface. We then report direct and indirect methods to characterise the thickness and distribution of the lubricant layer. Finally, we examine how droplets interact with LIS and the unique properties afforded by the lubricant before providing an outlook into where research centred on understanding the lubricant layer is heading in the new decade.

1. Introduction

Liquid-infused surfaces (LIS) are structured surfaces that are infused with a layer of a viscous liquid, which creates a smooth interface on which most immiscible liquids can flow without sticking or spreading. Since LIS were first introduced in 2011,[1, 2] they have expanded to take an essential role in the literature on omniphobic and special wettability surfaces. The reason they have attracted such great attention in a relatively short amount of time is that they offer a rich platform for studying wetting and flow at complex and responsive interfaces. They also offer a wide range of attractive properties in applications, including anti-biofouling in both medical and marine environments, drag-reducing properties, anti-icing properties and droplet manipulation. Several recent reviews have been dedicated to specific applications and properties of LIS[3-12] and methods of fabrication.[7, 13]

LIS outperform the other major family of non-wettable surfaces, superhydrophobic surfaces, in anti-fouling ability, anti-icing capabilities, and are comparable in drag reduction. LIS are not without fault, however, as the liquid nature of the lubricant makes them susceptible to depletion and degradation of properties. The lubricating layer is the crucial component that affords LIS their unique and favourable properties. However, its distribution and change over time are often overlooked in favour of the properties it imparts during the initial stages of operation. The choice of lubricant, its interaction with the substrate, and its interaction with its environment are integral to the success of LIS. As a result, detailed characterisation of the lubricant layer thickness and distribution overtime is needed to understand and improve the performance of a given system. Characterisation of lubricant layers presents several challenges due to their thin and dynamic nature. This review summarises the studies addressing these aspects and provides an outlook on outstanding problems in LIS relating directly to the lubricant layer.

First, we introduce liquid-infused surfaces and briefly mention manufacturing methods. Then we discuss trends of lubricant choice in the literature and rational choice of lubricant for a given system. Next, we look at how the infusion of lubricant onto the surface and how depletion of lubricant from the surface affects surface properties. Then, we examine reported techniques for characterisation of lubricant volume and distribution and their strengths and weaknesses. Finally, we discuss how external fluids interact with the lubricant layer and some of the unique properties that arise.

1.1. Liquid-infused surfaces (LIS)

The term liquid-infused surface (or lubricant-infused surface) (LIS) broadly covers all surfaces that have a layer of liquid on their surface and draw inspiration from the carnivorous *Nepenthes* pitcher plant.[1] This plant is known as a "pitfall" trap as it captures its prey (usually ants) by luring them to a slippery lip (known as a peristome) where they cannot grip and fall into the pitcher to be digested, see **Fig. 1**.[14] The slippery nature of the peristome is due to surface roughness trapping a thin

[a] *The School of Chemistry, The University of Sydney NSW 2006 Australia*
[b] *The University of Sydney Nano Institute, The University of Sydney NSW 2006 Australia*
[c] *Central Clinical School, Faculty of Medicine and Health, The University of Sydney NSW 2006 Australia*
[d] *The Heart Research Institute, Newtown, NSW 2042 Australia*
[e] *The Charles Perkins Centre, The University of Sydney NSW 2006 Australia*
* chiara.neto@sydney.edu.au

lubricating water film, inhibiting the interaction of the peristome with hydrophobic insect feet.[15] Similarly, a manufactured surface can take advantage of a trapped liquid film to impart desirable properties to the surface. Like the pitcher plant, the layer is lubricating and so allows for the surfaces to self-clean (provided the lubricant and the impinging fluid are immiscible). The layer presents a liquid surface, as opposed to a solid surface, significantly reducing the adhesion of any foulants. There are many ways to manufacture LIS, which we divide into three classes based on the length scale of the structure that traps the lubricant layer: 1-dimensional, 2-dimensional and 3-dimensional (see **Fig. 2C)**.

1.2. Classification and Manufacture of LIS

Manufacturing techniques have recently been reviewed,[7] therefore, we will only discuss the manufacture of LIS in broad terms.

1.2.1. 1-Dimensional LIS The first class of surfaces is called 1D LIS as the surface structure that retains the lubricant is on the molecular scale (e.g. of the order of a single to a few monolayers, see **Fig. 2C**). A thin layer of lubricant (thickness of the order of a few nm) is either stabilised through intermolecular interactions with a molecular monolayer bound to the solid substrate or is directly grafted to the solid surface. There are relatively few studies using this molecular infusion mechanism compared to manufacturing LIS through other means.

1D LIS are manufactured in two ways. In the first method, the lubricant is infused within a molecular layer grafted onto a solid substrate, to promote the adsorption of the lubricant on the substrate. These were first reported in academia as a modification of medical equipment with a perfluorocarbon molecular layer and then infusion with relatively small perfluorinated molecules, such as perfluorodecalin.[16, 17] The increased interaction of the perfluorodecalin with the perfluorocarbon modified substrate allows for the liquid to be stabilised and reduce the adhesion of thrombogenic molecules and cells. Industrially, perflourinated lubricants have been tethered to hard disk surfaces to increase lubricant retention[18] and thin polymer films used to immobilise silicone oil.[19] More recently, similar systems have been reported, but instead, use

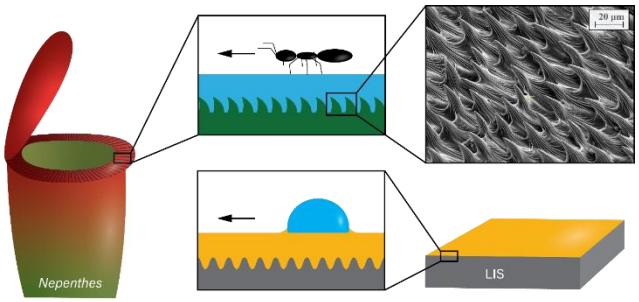

Fig. 1 – (Top) The Nepenthes pitcher plant traps a thin layer of water in its peristome (through roughness, as shown in the scanning electron micrograph of the peristome of the pitcher plant), creating a slippery liquid layer and causing ants to slide into its pitcher where they are digested. (Bottom) LIS imitate this mechanism by trapping a lubricant layer on their surface (usually through roughness on different length scales) making them slippery to droplets and affording them numerous desirable properties.

polydimethylsiloxane (PDMS)/silicone oil combinations[20] or using π-π or π-COOH interactions to immobilise lubricants.[21-23] The second method to manufacture 1D LIS is to covalently attach long-chain molecules to the surface in such a way that they retain liquid-like features. This class of 1D LIS are known as Slippery Omniphobic Covalently Attached Liquid (SOCAL) surfaces[24] and has attracted much attention recently due to their potential to eliminate lubricant depletion. In this method, surfaces can be made to be slippery without having any liquid flowing, displaying very low contact angle hysteresis (< 1°).[25] Methods to create these surfaces include grafting PDMS chains to a silicon surface using heat[25, 26] or acid catalyst[27] growing PDMS chains from a surface[24, 28, 29] or grafting perfluoro-polymers[30] or polymer brushes to the surface.[26, 31, 32]

1.2.2. 2-Dimensional LIS The second class of surfaces is called 2D LIS, as the surface structure traps the lubricant by capillary action within nano- and micro-scale topographical features **(Fig. 2C**). This is by far the most common type of LIS reported in the literature and, in general, most of the work presented here refers to this type of surface. Intermolecular forces may aid in retaining a thin layer of lubricant on the tops of surface features, and therefore the study of short- and long-range interactions is critical .[1, 33-35]

2D LIS are manufactured by first creating roughness with the correct surface chemistry and then infusing a lubricant into the roughness (for recent reviews see[7, 13]). The important feature of this type of LIS is that there is roughness, ideally on the nanoscale,[36] and that the surface is of the correct chemistry to repel fouling liquids.[37] The factors determining the correct chemical combination of surface and lubricant are explored in **Section 2.2.** The underlying substrate can be inorganic or organic, so long as the surface can be functionalised to allow for successful infusion.

1.2.3 3-Dimensional LIS The third class of surfaces is called 3D LIS, as the inherent porosity of a 3D molecular network is used to trap and store lubricant. Here, compared to 2D LIS, an additional mechanism is acting with the storage of lubricant driven by an increase in entropy gained from the swollen state of the polymer.[38] In this system, the lubricant is absorbed into a polymer or other material network of the correct chemistry and then leaves a lubricious overlayer on the surface. Although intermolecular forces are the only stabilising force for the liquid overlayer, lubricant held in the bulk can replenish lubricant lost on the surface. These surfaces are also known as organogels,[39] and have been previously studied in a number of applications.[40, 41] Exploiting their ability to excrete a lubricating layer for anti-adhesive properties is novel.

3D LIS require a polymer that can be swollen by the lubricant. The most common of these is PDMS soaked in silicone oil (known as iPDMS). The silicone oil swells the PDMS matrix through diffusion and forms a lubricious overlayer which is later excreted whenever the overlayer is removed.[38] Other polymer matrices have also been employed such as polyvinylidene fluoride (PVDF)[42, 43] and polyethylene[44]. Surfaces of this type draw inspiration from the mucous-excreting glands of toads that cause the animal to be covered in a protective mucous layer that is constantly replenished from said glands. These

surfaces have even been produced with macroscopic cavities filled with lubricant that mimic the glands.[45] PDMS has also been successfully swollen with alkanes, [46] and fatty acids.[47] An alternative approach blends the PDMS precursor with the lubricating liquid before crosslinking the PDMS, allowing the lubricant to be excreted later due to syneresis.[48] Industrially, this form of lubrication has found application in a medical field

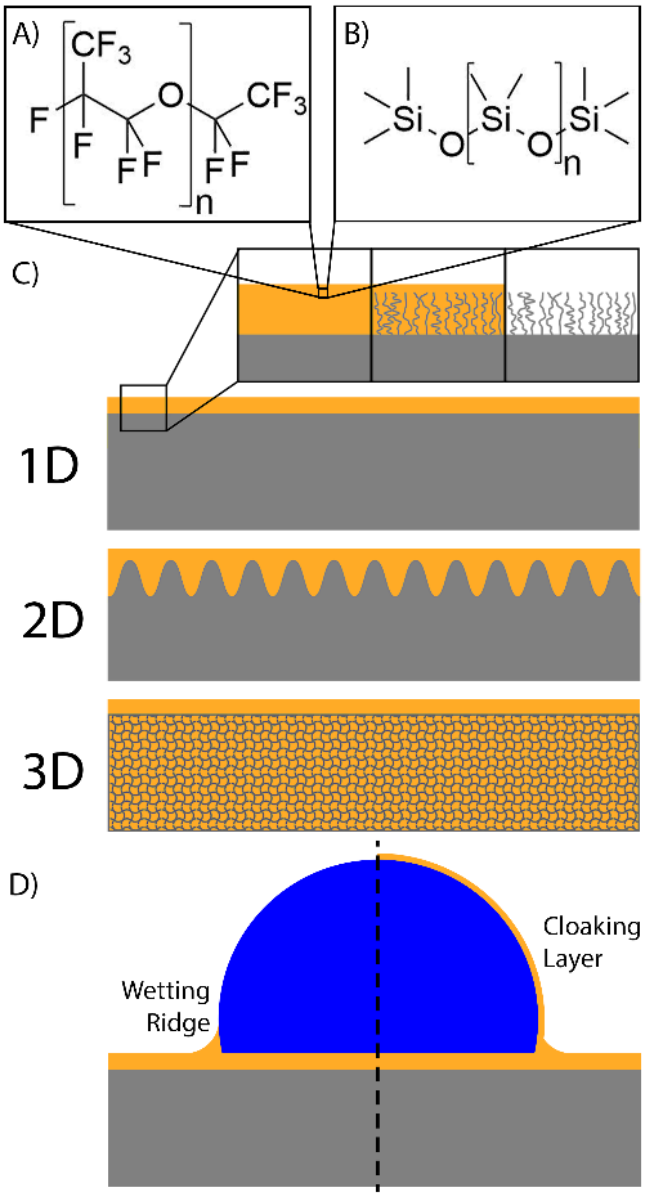

Fig. 2 – Lubricants used in LIS are most commonly A) perfluoropolyethers (PFPEs) or B) polydimethylsiloxane (PDMS), also known as silicone oil or dimethicone. C) We categorise LIS into three broad classes based on how they trap lubricant (yellow colour) on the surface: 1D, 2D and 3D. Images not to scale. D) Morphology of a water droplet (blue colour) on a LIS – lubricant is drawn up into an annular wetting ridge around the base of the droplet (left side of the droplet); the droplet may be covered by a thin cloaking layer of lubricant (right side).

where thin layers of PDMS are used to stabilise silicone oil or other lubricants on medical devices.[49-51]

2. Lubricant choice

The choice of lubricant is essential to ensure that the resulting infused surface has desirable properties. The very first reports of LIS both discussed lubricant choice. Lafuma and Quéré[2] outlined the requirements for a liquid-infused rough surface to repel water in particular, and they highlighted the importance of ensuring that lubricant infuses into the solid, is immiscible with water to ensure it is repelled, and water does not sink through the lubricant to contact the solid surface. Wong *et al.*[1] also outlined three general criteria for successful design:

1. The lubricating liquid must wick into, wet and stably adhere within the substrate.
2. The solid must be preferentially wet by the lubricating liquid rather than the liquid that is to be repelled (working fluid).
3. The lubricating and working liquid must be immiscible.

With these basic requirements in mind, it is clear that there is no *ideal* choice of lubricant for all situations, but instead the choice of lubricant is dependent on the application of the surface. In general, lubricants tend to have the following properties:

1. Low surface tension (< 30 mN m^{-1}), as to easily spread on most surfaces and infuse into roughness.
2. Low vapour pressure (< 1 Pa), as to not be quickly lost through evaporation.
3. Chemical inertness, as to not be easily degraded when in contact with other chemicals.
4. Wide range of viscosity, but most common < 100 cSt; not too low to delay lubricant depletion but not too high to accelerate lubricant infusion.

As many applications for LIS will inevitably release lubricants into the environment, their environmental impact is an important consideration that is generally not covered in the literature. Here we review the literature to assess the potential effects from lubricant release and suggest less impactful alternatives in **Section 2.4.**

2.1. Trends in reported lubricants

Two main classes of lubricant dominate the literature on LIS: perfluoropolyethers (PFPEs) and linear polydimethylsiloxane (PDMS, also known as silicone oil or dimethicone; here we refer to linear PDMS as silicone oil). PFPEs are a class of perfluorinated compounds whose general structure is shown in **Fig. 2A**. They have been used as lubricants in the aerospace industry for decades and are known for their chemical inertness, low surface tension and (in the longer chain length molecules) low vapour pressure.[52] The most common type of PFPE employed is the Krytox series of lubricants from Dupont, marketed for aerospace applications. Similarly, silicone oil is known for its chemical inertness, low surface tension and low vapour pressure and is often used to lubricate mechanical devices with its structure shown in **Fig. 2B**. These properties, along with their relatively low cost compared to PFPEs,[52] make silicone oil ideal for use in LIS. **Table 1** details the variety of PFPEs and silicone oil used along with their physical properties, and the publications that use them. Lubricants other than PFPEs and silicone oil are listed in **Table 2**.

As shown in **Table 2**, other lubricants include those from highly available sources such as vegetable oils,[44, 67, 70, 171-173] polyols,[163, 174] or even motor oil.[171] Edible lubricants enable the application of LIS in areas of food handling and processing,[175] while cheaper oils pave the way for scalability of LIS manufacture in large scale applications.

Ionic liquids have also been successfully used as lubricants[37, 43, 111, 176-182]. Ionic liquids have negligible vapour pressure,[37] but the molecular composition has to be modified to make them hydrophobic and repellent to water and, as such, all reported ionic liquids include a fluorinated anion.

While most of LIS applications seek to repel aqueous foulants and, as such, employ hydrophobic lubricants, specific applications can call for the use of hydrophilic lubricants.[1, 32, 35, 67, 80, 144, 163, 174, 183, 184] One example of a situation where infusion of a hydrophilic liquid is beneficial is repelling oil underwater. In this case, the underlying surfaces are superhydrophilic and infused with water.[35, 184] Hydrophilic lubricants have also been employed on anti-icing surfaces with Ozbay *et al.* showing that an 85% solution of glycerol infused into hydrophilic filter paper reduces ice accretion much more effectively than a hydrophobic lubricant infused into a hydrophobic filter paper.[163]

For many of these lubricants, a major concern is chemical stability. Long term application of LIS requires the lubricant to be stable over a long period. While some may have beneficial environmental or medical properties (see **Section 2.4** and **Section 2.5**), this often comes at the cost of chemical stability. For example, plant oils lose around 30% of their oxidative stability after 12 months storage.[185]

A wide range of viscosity values are reported, between 1 and 20,000 cSt. Most viscosity values used are below a few hundred cSt, to make infusion easier, as the lubricant needs to flow into the surface structure or into a 3D matrix. Higher viscosities reduce the speed at which the lubricant depletes from the surface but decrease the mobility of droplets or other foulants on the surface (**Section 6.3**). Similarly, a wide range of vapor pressure values are used, although lower vapor pressure values are preferred. Low vapor pressures ensure that lubricants do not evaporate under ambient conditions, but this is not a necessity for applications where the surface is submerged in a closed system. For example, perfluorodecalin has a relatively high vapor pressure of 880 Pa, but is useful in situations where the liquid cannot evaporate such as the closed system of an implanted medical device[186] or a semi-closed system where air exposure is minimal, e.g. extracorporeal circuits or catheters.[16,

Table 1 – Properties of the different Krytox and silicone oil lubricants used in LIS research. Properties are taken from manufacturer data sheets, MSDS or reporting reference.

Lubricant	Density (g cm^{-3})[a]	Lubricant/ Air Surface Tension (mN m^{-1})[a]	Viscosity (cSt)[a]	Vapor Pressure (Pa)[a]	Used in References
Krytox Series					
Krytox 100	1.87	16-20	12.4	-[c]	53-78
Krytox 101	1.89	16-20	17.4	-[c]	79-83
Krytox 102	1.91	16-20	38	-[c]	59, 84-86
Krytox 103	1.92	16-20	82	-[c]	8, 74, 87-105
Krytox 104	1.93	16-20	177	-[c]	55, 63, 86, 106
Krytox 105	1.94	16-20	522	-[c]	46, 55, 74, 86, 89, 90, 107-109
Krytox 106	1.95	16-20	822	-[c]	55, 70, 86
Krytox 143 AZ	1.91	16-20	40	500	55, 110
Krytox 1506	1.88	-[c]	60	$5x10^{-5}$	62, 111-113
Krytox 1514	1.89	18	140	$2x10^{-5}$	70
Krytox 16256	1.92	19	2560	$4x10^{-12}$	70
Silicone Oil					
3 cSt	0.90[b]	19	3	<700	38, 114
5 cSt	0.91[b]	20	5	<700	48, 60, 115-122
10 cSt	0.93[b]	20	10	<700	33, 38, 59, 115, 121, 123-137
20 cSt	0.95[b]	21	20	<700	59, 83, 105, 117, 121, 134, 138-145
40 cSt	0.95[b]	21	40	<700	12, 20, 59
50 cSt	0.96[b]	21	50	<700	59, 115, 117, 121, 134, 146-150
100 cSt	0.96[b]	21	100	<700	60, 76, 117, 121, 134, 139, 142, 144, 150-159
350 cSt	0.97[b]	21	350	<700	131, 132, 160-168
500 cSt	0.97[b]	21	500	<700	131, 134, 150, 156, 157, 169
1,000 cSt	0.97[b]	21	1,000	<700	60, 76, 121, 128, 142, 156, 157, 170
10,000 cSt	0.97[b]	22	10,000	<700	121, 132, 142
20,000 cSt	0.97[b]	22	20,000	<700	132
100,000 cSt	0.97[b]	22	20,000	<700	121

[a] at 20 °C, unless specified otherwise, [b] at 25 °C, [c] unavailable

[17] Perfluorodecalin is suited for biomedical LIS based on its prior use in medicine and existing clinical safety data.[9] The complexity of LIS applied to medical devices and the choice of lubricant from a clinical safety perspective are discussed in further detail in **Section 2.5.**

PFPEs and silicone oil have unique chemical composition, leading to the favourable properties that make them popular lubricants. In perfluorinated compounds the carbon-fluorine (C-F) bond is one of the strongest chemical bonds, due to the high electronegativity of fluorine that gives the bond a partial ionic character.[239] Multiple fluorine atoms bonded to the same

Table 2 – Reported lubricants used in LIS research and their properties (other than Krytox and silicone oil lubricants). Properties are taken from manufacturer data sheets, MSDS or reporting reference.

Lubricant	Density (g cm^{-3})[a]	Lubricant / Air Surface Tension (mN m^{-1})[a]	Viscosity (cSt)[a]	Vapor Pressure (Pa)[a]	Used in References
Perfluorinated compounds					
FC-43	1.86	16	2.5	192	79, 187
FC-70	1.94	18	12	15	1, 63, 163, 176, 179, 188-192
Fomblin Y	1.88-1.90	21-22	38-470	$8x10^{-6}$ - $2x10^{-4}$	183, 193-198
Fomblin YR	1.91	24	1200		199-201
Perfluorodecalin	1.92	17.6	5.10	880	16, 91, 186, 202
Perfluoroperhydrophenanthrene (Vitreon)	2.03	19	28.2	< 100	17, 131, 186, 203, 204
Unspecificed PFPE	-[e]	-[e]	-[e]	-[e]	205-211
Silicone compounds					
Tetramethyltetraphenyl trisiloxane (DC-704)	1.07	37	38	< 0.1	212
Decamethylcyclopentasiloxane (D5)	0.96	19[b]	4	20[b]	163
Unspecified Silicone Oil	-[e]	-[e]	-[e]	-[e]	212-222
Ionic liquids					
1-butyl-3-methylimidazolium bis(trifluoromethylsulfonyl)imide	1.44	33	50	< 0.01	37, 111, 176-179, 182, 223
1-octyl-3-methylimidazolium hexafluorophosphate	1.30	33	34	< 0.006	177
1-ethyl-3-methylimidazolium bis(trifluoromethylsulfonyl)imide	1.53	35	35	-[f]	178, 181
1-hexyl-3-methylimidazolium bis(trifluoromethylsulfonyl)imide	1.37	55	31	-[f]	178
Plant Oils[c]					
Canola Oil	0.91	32	78	< 13	171, 224
Coconut Oil	0.92	18	23	-[f]	171
Olive Oil	0.91	32	75	-[f]	67, 171, 224
Almond Oil	0.92	-[f]	-[f]	-[f]	173
Carnation Oil	0.92	-[f]	-[f]	-[f]	70
Cocoa Oil	0.92	-[f]	-[d]	-[f]	172
Cottonseed Oil	0.92	35	73	-[f]	44
Soybean Oil	0.92	34	59	-[f]	44, 175
Other lubricants					
Mineral Oil	0.85	30	10, 68	< 1	44, 81, 97, 105, 124, 125, 225, 226
Decanol	0.83	29	12[b]	1	176
Ethylene Glycol	1.12	48	16.9[b]	8	163, 174, 227
Triethylene Glycol	1.13	46	49[b]	< 1	174
85% Glycerol	1.23	65	1300	900	163
Kerosene	0.80	23-32	1.64[b]	282	191
Motor Oil	-[e]	-[e]	-[e]	-[e]	171
Oleic Acid	0.90	33	27.64[b]	1253	22, 23, 47, 174
Methyl Oleate	0.87	29[b]	6.39	$5.4x10^{-4}$[b]	47
Ethyl Oleate	0.87	28	6.9	$4x10^{-4}$[b]	98, 109, 175
Ferrofluid	-[e]	-[e]	-[e]	-[e]	228-231
Paraffin Wax	0.90	30	-[d]		98, 218, 232-238
Thermotropic Liquid Crystal	-[f]	-[f]	-[f]	-[f]	171
Water	1	72	1	2339	1, 32, 35, 67, 80, 86, 163, 183, 184

[a] at 20 °C, unless specified otherwise, [b] at 25 °C , [c] properties vary with sample as plant oils are variable mixtures, [d] solid at 20 °C, [e] varies, [f] unavailable

carbon increase this effect as there is a higher partial positive charge on the carbon. Fluorine has very low polarisability, meaning that compounds that contain a lot fluorine have very weak London dispersion force interactions.[239] This means that although perfluorinated compounds are non-polar, they are lipophobic in addition to being hydrophobic. As a result, they are immiscible with almost all organic solvents. The weak intermolecular forces give perfluorinated compounds low surface tension and a low viscosity (compared to polymers with similar boiling points). Silicone oil is comprised of a backbone of siloxane bonds (-Si-O-Si-) with methyl groups attached to the silicon atoms. The combination of the partially ionic siloxane bond (about 40%, due to the low electronegativity of silicon[240]) and the low polarity methyl groups gives silicone oil a unique chemical character, compared to organic polymers. Its chemistry is neither purely hydrophilic, nor purely hydrophobic, nor is it a surfactant as there is not enough separation between the hydrophilic and hydrophobic portions. Rearrangement of chains so that the methyl groups are at the surface gives silicone oil an overall macroscopic hydrophobic character.[241] The large Si-O-Si bond angle (151.2°[240]) and large Si-O bond length (1.63 Å[240]) gives a small torsional barrier for rotation about the backbone and a very low T_g (150 K[241]). The partially ionic nature of the siloxane bonds combined with high bond energy (445 kJ mol^{-1} [241]) gives silicone oil excellent chemical and thermal stability, while weak intermolecular interactions between the methyl groups give low surface tension.

2.2. Rational lubricant choice

Correct lubricant choice is dependent on several variables such as substrate and application. Some publications have attempted to formalise frameworks for lubricant selection and are reviewed here.

Wong *et al.* use interfacial energies to describe a stable infused state - one where the solid is preferentially wet by the lubricant rather than the liquid to be repelled (working fluid).[1] By considering three wetted states (working fluid wetting the substrate, lubricant wetting the substrate, and working fluid on top of the lubricant) and ensuring that the first state is always energetically less favourable than the other two states, they propose two conditions that describe a stable infused state:

$$R(\gamma_l \cos\theta_l - \gamma_d \cos\theta_d) - \gamma_{ld} > 0$$

$$R(\gamma_l \cos\theta_l - \gamma_d \cos\theta_d) + \gamma_d - \gamma_l > 0$$

Where the R is the roughness factor (actual surface area to projected surface area), γ_l, γ_d are the interfacial tension of lubricant/air and impinging droplet/air, respectively, γ_{ld} is the interfacial tension between the lubricant and impinging droplet and ϑ_l, ϑ_d are the static contact angles of the lubricant and droplet on the flat substrate. This framework correctly predicts several stable lubricant/substrate combinations.[1]

Using classic liquid wetting behaviour, Smith *et al*. identified two key features of the lubricant layer that appear when droplets interact with LIS: the wetting ridge and the cloaking layer (See **Section 6** and **Fig. 2D** for more information).[37] The wetting ridge is an annular ridge of lubricant pulled up around the droplet due to the out-of-plane component of the surface tension at the droplet contact line, acting on the lubricant. Such a wetting ridge is similar to the ridge seen around droplets placed on soft or elastic surfaces.[242] The cloaking layer is a direct result of the spreading parameter of the lubricant on the water droplet. The spreading parameter for the lubricant over water is $S = \gamma_{wa} - \gamma_{la} - \gamma_{wl}$ where γ_{wa} is the interfacial tension between water and air, γ_{la} is the interfacial tension between lubricant and air and γ_{wl} is the interfacial tension between water and lubricant. If $S > 0$ (for example for silicone oil spreading over water S = 73 -21-35 = 17 mN/m), then a thin layer of lubricant will spontaneously cloak the droplet as this lowers the overall energy of the system.[37]

A positive spreading parameter over the substrate is also required for the lubricant to spread and cover the topography. Using the Young-Dupré equation, $S = \gamma_{lw}(\cos\vartheta_o - 1)$, where γ_{lw} is the surface tension of lubricant in the medium (water) and ϑ_o is the static contact angle of the lubricant on the substrate in the medium. If $\vartheta_o = 0$, the lubricant spreads on the surface and covers high topographical regions even when the overall lubricant level is below these features. Smith *et al.* showed this using laser scanning confocal microscopy and environmental scanning electron microscopy (see **Section 5** for more details) for lubricants with different spreading parameter. For the fully wetting case, they used silicone oil, and for the partially wetting case, they used an ionic liquid (1-butyl 3-methylimidazolium bis(trifuoromethylsulfonyl) imide – BMIm). Their results show that the lubricant coats the tops of hydrophobized silicon microposts for silicone oil, but not for BMIm. The authors then examine all the possible thermodynamic configurations for a solid/lubricant/air and solid/lubricant/water system as these represent the majority of wetting scenarios LIS will face, as in **Fig. 3A**. The stability of a lubricant layer on a surface often changes when the surface is moved from air to another medium, e.g. underwater. A surface with a stable lubricant layer in air may result in water droplet pinning if the lubricant dewets under the droplet and the droplet can penetrate the surface texture. An example of this is a hydrophilic substrate infused with a hydrophobic lubricant on which a water droplet is placed: the water will cause the lubricant to dewet and will sink into the lubricant layer, contacting the surface and pinning.[133] These wetting states have been verified computationally.[243]

For a stable LIS, the solid must be preferentially wetted by the lubricant and not by the working liquid to be repelled. The surface of common substrates that are hydrophilic, such as untreated ceramics or metals, needs to be modified to make them more amenable as LIS, for example through silanisation.[37, 66, 132, 209, 212]

This framework of considering the interfacial tensions of the system cannot account for all observed wetting phenomena on LIS. Rowthu *et al.* found that this framework could not predict the stability of a hexadecane droplet on PFPE-infused alumina surfaces and instead built a model that takes into account density, viscosity, capillary time, capillary height, van der Waals forces of attraction, evaporation rate, surface diffusivity and

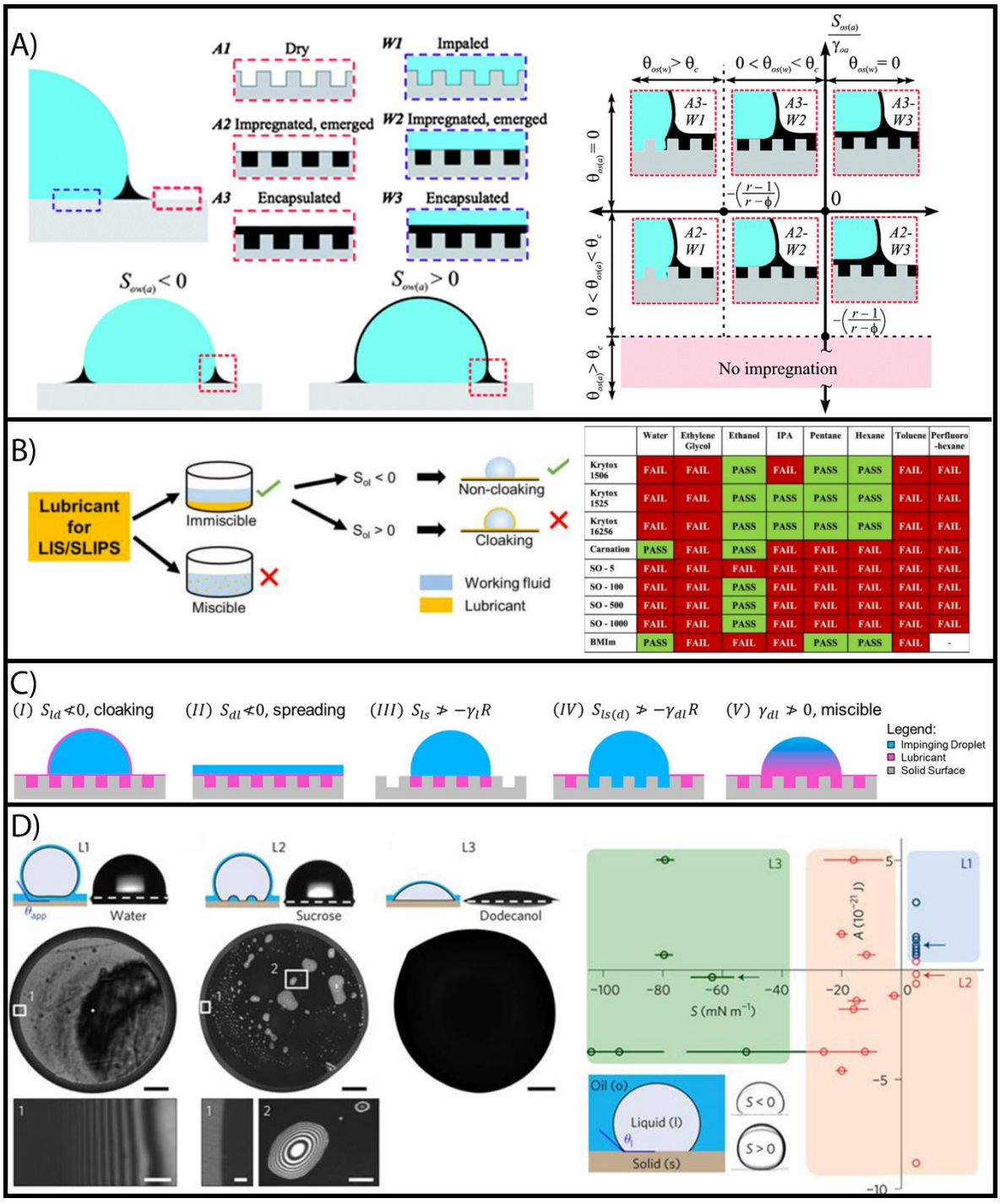

	Water	Ethylene Glycol	Ethanol	IPA	Pentane	Hexane	Toluene	Perfluoro-hexane
Krytox 1506	FAIL	FAIL	PASS	FAIL	PASS	PASS	FAIL	FAIL
Krytox 1525	FAIL	FAIL	PASS	PASS	PASS	PASS	FAIL	FAIL
Krytox 16256	FAIL	FAIL	PASS	PASS	PASS	PASS	FAIL	FAIL
Carnation	PASS	FAIL	PASS	FAIL	FAIL	FAIL	FAIL	FAIL
SO - 5	FAIL	FAIL	FAIL	FAIL	FAIL	FAIL	FAIL	FAIL
SO - 100	FAIL	FAIL	PASS	FAIL	FAIL	FAIL	FAIL	FAIL
SO - 500	FAIL	FAIL	PASS	FAIL	FAIL	FAIL	FAIL	FAIL
SO - 1000	FAIL	FAIL	PASS	FAIL	FAIL	FAIL	FAIL	FAIL
BMIm	PASS	FAIL	FAIL	FAIL	PASS	PASS	FAIL	-

Fig. 3 – A) The possible thermodynamic configurations of lubricant in air and underwater as outlined by Smith *et al.*[37] The lubricant cloaks the droplet on the surface, if the spreading parameter, S_{OW}, of the lubricant on the droplet is zero or positive. The wetting configuration is a function of the spreading parameter of the lubricant over the solid in air and water ($S_{OS(a)}$ and $S_{OS(w)}$, respectively). Adapted with permission from [37]. © 2013 Royal Society of Chemistry. B) The criteria outlined by Sett *et al.*[244] for lubricant stability on LIS with combinations of lubricants (subscript o) and impinging fluid (subscript l) that either pass or fail these criteria. Adapted with permission from [244]. © 2017 American Chemical Society. C) The possible failure modes outlined by Preston *et al.*[245] for a lubricant/substrate/droplet system. Adapted with permission from [245]. © 2017 American Chemical Society. D) The three wetting states presented by Daniel *et al.*[80] for a droplet on a LIS with a corresponding phase diagram as a function spreading parameter, *S*, and Hamaker constant, *A*. L1 is a stable lubricating layer, L2 is an unstable lubricating layer, and L3 is a non-existent lubricating layer. L1 scale bar: 0.1 mm, inset: 10 µm; L2 scale bar: 0.3 mm, inset 1: 15 µm, inset 2: 40 µm; L3 scale bar: 0.1 mm. Adapted with permission from [80]. © 2017 Nature Springer. Note that although Sett *et al.* and Preston *et al.* both state that a cloaking layer on a droplet is undesirable, this is only in the case for applications of LIS in heat exchangers and its existence does not contribute greatly to depletion compared to the wetting ridge.[59]

molecular shape and dimensions.[183] Using this extended framework, the authors could account for all observed wetting phenomena on their surface.

LIS are often touted to be omniphobic, but the stability and application of a surface is heavily dependent on the working fluid. Sett *et al.* outline a framework for optimal lubricant

performance where the lubricant is not miscible with the test fluid and the lubricant does not cloak a droplet of test fluid.[244] They tested these conditions on several lubricants and working fluid combinations and found that very few lubricants with higher surface tension, such as carnation oil and the ionic liquid BMIm, met their criteria of being immiscible with and not cloaking a water droplet. Their methodology and results are summarised in **Fig. 3B.** Their framework (and the framework presented next by Preston *et al.*) assumes that a cloaking lubricant is unfavourable as it adds an additional barrier between the droplet and vapor in heat exchange applications. This requirement is not a concern in other applications, where the cloaking layer only marginally increases lubricant lost, as far more lubricant is lost in the wetting ridge than in the cloaking layer.[59] As such, the presence of a cloaking layer is not necessarily a negative attribute when selecting a lubricant, but should be considered.

One fundamental weakness of considering only surface energy to determine the stability of LIS is that these values are not published for an arbitrary system.

Preston *et al*. use the van Oss–Choudary–Good equation[246] to predict surface energy and design LIS that can repel a given fluid.[245] Five criteria for failure of a LIS are identified from surface-energy-based reasoning (shown visually in **Fig. 3C**) and are:

1. $S_{ld} < 0$, the lubricant does not spread over the droplet – the droplet is not cloaked.
2. $S_{dl} < 0$, the droplet does not spread over the lubricant; it forms droplets that can be shed.
3. $S_{ls} > -\gamma_l R$, the lubricant spreads into the structural features of the substrate (of roughness factor R) in the presence of its vapor.
4. $S_{ls(d)} > -\gamma_{dl} R$, the lubricant does not spread into the structure of the substrate in the presence of the impinging droplet.
5. $\gamma_{dl} > 0$, the lubricant and the droplet are miscible.

Where subscripts *l, d, s* refer to lubricant, impinging droplet and substrate respectively; where S_{xy} represents the spreading parameter for x spreading over y and $R = (r-1)/(r-\phi)$ is a roughness factor calculated using the roughness, r, and the solid fraction, ϕ, and is 0 for a flat substrate and 1 for a very rough substrate.

By considering interfacial energy as the sum of dispersive and van der Waals interactions (Lifshitz-van der Waals (LW)) and the polar interaction (denoted as superscript + and -), the interfacial energy between two phases is:

$$\gamma_{AB}^{total} = \gamma_A^{LW} + \gamma_B^{LW} - 2\sqrt{\gamma_A^{LW}\gamma_B^{LW}} + 2\sqrt{\gamma_A^{+}\gamma_A^{-}} + 2\sqrt{\gamma_B^{+}\gamma_B^{-}} - 2\sqrt{\gamma_A^{+}\gamma_B^{-}} - 2\sqrt{\gamma_B^{+}\gamma_A^{-}}$$

These five criteria for failure can be used to assess the stability of a given substrate/lubricant/droplet system. Preston *et al.* correctly predict the failure mode of several solid/lubricant/droplet combinations from both their own experiments and ones reported in the literature. Their model can be used to rationally design a surface for a specific application.

For example, they predicted that a strong polar interaction between the substrate and the lubricant would allow a LIS to repel impinging droplets with surface tension of $\gamma \approx 11$ mN/m. They identified SiO_2 substrate and hexafluoroisopropanol (6F-IPA) lubricant as a candidate system and managed to repel butane ($\gamma \approx 13$ mN/m). Prior to this, the lowest surface tension reported to be repelled by LIS was pentane ($\gamma \approx 17$ mN/m).[1, 113]

Daniel *et al.* used nanoscale interactions to rationalise the wetting behaviour of a lubricant underneath a droplet. Accounting for van der Waals interactions, they built a phase diagram describing three lubrication states: stable, unstable (dewetted patches) and non-existent (denoted L1, L2, L3, respectively, see **Fig. 3D**).[80] Daniel *et al.* used interference microscopy (see **Section 5** for more details) to study the thickness distribution of lubricant underneath the droplet for 24 substrate/lubricant combinations and found for a stable and continuous lubricant layer, two criteria must be met: $S > 0$ and $A > 0$ (i.e. a lubricant that spreads on the surface and is stabilised by van der Waals interactions as indicated by a positive Hamaker constant, A). Without the stabilising van der Waals interaction, the droplet will contact the surface as the lubricant layer is squeezed out due to Laplace pressure from the droplet's curvature.[80, 247] If the droplet does contact the substrate, this does not preclude the droplet from moving easily, with droplets in both L1 and L2 wetting states leading to oleoplaning on the substrate. For the L1 state, this occurs at any velocity, but only occurs after a threshold velocity for L2.[80] Like the spreading parameter, the Hamaker constant is often not useful for designing LIS *a priori* as it is difficult to estimate correctly for complex multi-component systems. Unknown Hamaker constants can be estimated using combinations of known Hamaker constants for single material systems.[248]

2.3. Multifunctional surfaces

An emerging field within LIS research is multifunctional surfaces, whereby the slippery functionality of LIS is combined with another functionality.

There are relatively few publications in this area, despite it being highly interesting and potentially useful. Some studies into multifunctional slippery surfaces achieve the extra functionality through functionalisation of the underlying substrate in 2D LIS.[203, 204, 249, 250] In this case, the lubricant not only mediates the interaction of any foulant with the surface, but also mediates the function of the added functionality. As a result, lubricant choice has the added dimension of ensuring that the selected lubricant allows for this extra functionality. Examples of added functionality are tuneable cell adhesion,[203, 204] incorporation of anti-microbial agents to inhibit bacterial/fungal growth,[250] and excretion of quorum sensing inhibitors to disrupt bacterial settlement.[249] In these cases, lubricants such as silicone oil and Vitreon allow for this added functionality.

The other common way of creating multifunctional LIS is to incorporate functionality into the polymer portion of 3D LIS.[213, 251, 252] In this case, it is less clear if the functionality lies in the underlying substrate or the lubricant due to their chemical

similarity. Example of functionality here include incorporation of nitric oxide (NO) donors to inhibit bacterial biofouling,[213] and controlling droplet motion using DNA.[251, 252]

The lubricant mediates any effects between foulants and the underlying substrate, so it is logical that functionality is added to the lubricant itself. However, examples of this are rare, with our search of the literature only finding ferrofluid-based LIS as an example of a multifunctional lubricant.[228-231] This apparent lack of functional lubricants reported in the literature makes this an exciting area for further study. One possible explanation for the lack of modified lubricants is the chemical inertness and chemical incompatibility of the most common lubricants with functional molecules. Both silicone oil and PFPEs do not easily lend themselves to chemical modification of the backbone and are not very good solvents for most molecules (which is also the reason they are popular lubricant choices, see **Section 2.1**).

Although solid lubrication is attracting much attention in the field of tribology,[253, 254] it is yet to make an appearance in LIS research. Solid lubrication is based on two-dimensional molecular sheets that have weak basal interactions allowing them to slide past one and other easily. Solid lubricants cannot replace liquid lubricants in LIS as LIS rely on the high mobility of a liquid surface. Instead, they may be able to impart some of their properties on liquid lubricants. There is evidence that the addition of two-dimensional flakes of graphene or molybdenum disulphide (MoS_2) added to oils greatly increases their stability at high temperature and improves their friction-reducing capabilities.[253-255] Addition of two-dimensional nanomaterials to lubricants for use in LIS may add benefits such as increased mobility or performance at high temperatures.

2.4. Environmental factors in lubricant choice

The most used lubricants, PFPE and silicone oil, are used in part for their chemical inertness. This inertness makes them ideal for broad application as they do not degrade due to reaction with foulants, or exposure to high temperatures (up to 300 °C in oxidative environments[256]). However, this inertness raises possible environmental concern as there are no natural pathways for degradation.

Although the first commercial anti-fouling paints based on LIS technology first went on sale in late 2019 (SLIPS N1x from Adaptive Surface Technology Pty Ltd[257] using a fluorinated PDMS-based lubricant), silicone antifouling paints with added oils for lower foulant adhesion have been used for decades.[258-261] These antifouling paints are very similar to the 3D LIS described above, with a PDMS (or similar) matrix swollen with up to 20 % w/w with an oil.[260] Although the presence of a lubricious overlayer was never confirmed in these studies, the antifouling behaviour of these surfaces is likely due to an immobilised and replenishing lubricant layer.

As a result of these existing antifouling technologies, there has been some concern surrounding silicone oil release into marine environments.[262] Silicone oil and other hydrophobic polymers are generally not bioactive owing to their hydrophobicity and high molecular weight.[263, 264] This means that they do not interact with biological systems and also do not bioaccumulate in marine organisms.[263-266] In addition, many researchers have shown that their lubricants are not biocidal.[55, 77, 125, 126, 133, 209] Instead, silicone oil released in the environment tends to coat particulate matter and end up in sediments.[263] While this is not a concern in low concentrations, in higher concentrations these oils have the potential to suffocate and damage marine organisms in a similar way to petroleum oil spills. Given the enormous volume of the ocean, this is unlikely to pose a threat in areas other than high traffic shipping lanes.[262] It is also believed that the potential damage from silicone oil in marine antifouling coating is far less than that from biocidal antifouling solutions,[262] such as the banned tributyltin (TBT) containing paints that bioaccumulate and were hugely damaging to shellfish populations.[267]

Although there is no clear data on the fate of PFPE in the environment, it is expected to be different from that of perfluorocarbons (PFCs) more generally. Most of the serious environmental concerns around the release of PFCs in the environment involve perfluorinated acids, which bioaccumulate in fish.[268] Bioaccumulation of perfluorinated acids is due to the presence of polar groups, which are not present in PFPEs. Due to their similar physicochemical properties, PFPEs likely face a similar fate as silicone oil, that is they are inert but could potentially lead to suffocation upon coating.

More generally, PFCs are well known environmental pollutants. Shorter chain PFCs are targeted for reduced use under the Kyoto Protocol of the United Nations Framework Convention on Climate Change due to their greenhouse gas potency.[269, 270] Lower molecular weight PFPEs can volatilize into the atmosphere, with typical boiling points ranging between 55 – 270 °C.[271] Combined with their long atmospheric lifetimes, the use and disposal of PFPEs should be considered before widespread usage. Much of the research into LIS for medical applications have used perfluorodecalin as the lubricant (see **Section 2.5**). The atmospheric lifetime of perfluorodecalin has been predicted to be around 1000 years with a solar heat-trapping potential that is 7200 times greater than CO_2. However, the very low concentration of perfluorodecalin in the atmosphere makes their contribution to climate change, so far, trivial.[272, 273] Like PFPEs, perfluorodecalin does not pose an immediate environmental risk, but its environmental impact should be considered before widespread usage.

The cosmetics industry is leading the way in finding replacements for silicone oil and other lubricants, due to consumer concerns around the environmental safety and the high carbon footprint of the production of synthetic oils.[274] In recent years, as many as 56% of all new shampoos are marketed as not containing silicone.[274] This is partly due to cyclic silicones (octamethylcyclotetrasiloxane (D4) and decamethylcyclopentasiloxane (D5)) being ruled as environmentally damaging[275] and consumers rejecting all silicone as a result. Some examples of replacements include isoamyl laurate,[276] diheptyl succinate and capryloyl glycerin/sebacic acid copolymer,[277] alkanes (C13-15),[278] or plant oils such as argan oil, castor oil or coconut oil.[279] Coconut oil has already been successfully employed as a lubricant[171] along with several other plant oils (see **Table 2**) and so it is likely that castor oil and argan oil can be used. These plant oils are mixtures of

fatty acids (such as oleic acid, which has also been successfully used as a lubricant, see **Table 2**), making mixtures of fatty acids (and their esters) suitable candidates as replacement for PFPEs and silicone oil,[47, 280] requiring further exploration. In addition, plant oils show inherent anti-microbial activity.[281-283]

2.5. Medical factors in lubricant choice

In recent years, liquid-infused surfaces have been investigated as coatings for medical devices such as those used in cardiovascular disease treatment and management.[4, 9] Their ability to repel complex biological fluids, such as blood, has made LIS a promising advancement for antithrombotic materials. This section provides a brief summary of rational lubricant choice for LIS in biomedical applications. We direct readers to other recently published reviews for more thorough coverage of LIS for clinical and biomedical applications.[4, 9]

In addition to the general criteria outlined in **Section 2.2** for successful LIS design, for medical applications, the infusing liquids must also be biocompatible. Key criteria to be considered in the choice of lubricant in LIS for medical and clinical applications have been suggested by Mackie *et al*.[9]:

1. Cytotoxicity towards human cells and environmental toxicity. Pharmaceutical grade liquids are essential.
2. Stability and longevity of the lubricant in the host environment in which the LIS is to be used, particularly against exposure to physiological flow of biological fluids such as blood.
3. Effects of any leached products, by-products, and biological clearance mechanisms, cost and feasibility of manufacture, sterilization and storage.

Silicone oils and fluorinated liquids are already in common use for biomedical applications with liquids from both classes approved by the US Food and Drug Administration (FDA) for vitreoretinal surgery.[284] Silicone oils are also used as lubricants for plastic syringes.[9, 285] Perfluoroperhydrophenanthrene (PFPH or Vitreon) and perfluorodecalin (PFD) have previously been demonstrated to be safe in human studies as an intraoperative and post-operative tool in the management of retinal tears.[286, 287] Similarly, PFD and Vitreon have been studied in human clinical trials as a tamponade agent in retinal detachment surgery.[288-290] PFD and perflubron (1-bromo-perfluorooctane) have also been evaluated in preclinical studies as blood substitutes, being emulsified and directly administered intravenously into the bloodstream.[291-293]

Based on their extensive clinical use as blood substitutes, the perfluorocarbons Vitreon and perflubron, appear not to bioaccumulate. Instead, they are phagocytosed by reticuloendothelial macrophages of the immune system and exhaled from the lungs.[284, 291, 292, 294] Mild flu-like symptoms and decreased platelet counts (by only 12-15%) were temporary in patients receiving blood substitutes and were proposed to be due to stimulation of the reticuloendothelial system.[284, 291] Concern over complement activation of blood substitute emulsions was found to be caused by the Pluronic F-68 stabilising agent, not the perfluorocarbons themselves.[9, 284, 291, 295, 296]

In contrast, pre-clinical and clinical studies of Krytox (PFPE) have not yet been reported. While PFPE-infused LIS were reported to not affect the macrophage viability on infused substrates[186] or cellular metabolism in 5% v/v Krytox in cell culture medium,[55] concentrations beyond 10% v/v significantly decreased cellular metabolic activity (fibroblasts). However, it is unclear if the toxicity is a result of lubricant blocking nutrient uptake and waste removal of the cells, or if the lubricant contained impurities (as Krytox lubricants are not accredited medical grade).

Silicone oil use in syringes has been associated with protein aggregation in biological drugs; however, it was shown that silicone oil is unlikely to be the cause.[297] A combination of protein biophysical properties, drug/protein formulation, stress conditions (flow out of the syringe) are likely responsible.[297] Like PFCs, small volumes of silicone oils injected subcutaneously are also recognised by reticuloendothelial macrophages, but the clearance mechanism is less well understood.[298] Recently, concern has been raised due to the increasing incidence of silicone embolization syndrome, which is a consequence of illicit use of large volumes of subcutaneous silicone injections for body enhancement. Unintended administration of silicone oil into the bloodstream in these procedures has caused adverse events, for example, embolization in distal organs such as the lungs, resulting in fatalities.[298, 299] The FDA has warned against using large volumes of silicone oil for these purposes and has only approved it for intraocular ophthalmic use.[300] Silicone oil introduced into the body via LIS would likely not be in large enough volume to cause the adverse effects reported in these cases. Nevertheless, the inflammatory response and clearance mechanisms of lubricant in tissue or the bloodstream needs further investigation to determine the safety of silicone oil in LIS-based medical devices. This highlights the importance of understanding the lubricant effect on the host environment and lubricant depletion mechanism (see **Section 4**).

PFC liquids such as PFD and Vitreon are advantageous lubricants in LIS for medical applications given their extensive clinical use and well-understood metabolic clearance mechanisms, as compared to other classes of liquids such as silicone oils. Further research and characterisation of biological interactions of other novel lubricants (e.g. edible plant oils, see **Table 2**) should be explored to determine if they are desirable for use in medical LIS. For all lubricants, it is necessary to characterise immune cell activation and bioaccumulation/clearance mechanisms and to conduct toxicity studies. It is also important to assess any application-specific characteristics, for example, coagulation, platelet and complement activation for blood-contacting medical devices.

3. Lubricant infusion and control over initial thickness

The performance of LIS is directly related to the distribution of lubricant on the surface and is influenced by the method of infusion and any subsequent treatments. For some types of 1D or 3D LIS, infusion of lubricant is an integral part of the manufacturing process and so little variation is possible. For 2D LIS, infusion is generally a separate step in sample preparation, and so the infusion method can impact sample performance.

This section reviews how different methods to infuse LIS during preparation impact their performance and how sample performance is tested following depletion.

3.1 Sample preparation

Although it might seem secondary to other considerations (such as lubricant/substrate combination), the method of infusing the lubricant into the substrate influences how much lubricant is present and, by extension, the surface's properties. Similarly, controlled depletion of lubricant is essential to produce substrates with consistent properties for testing.

As lubricants and substrates vary widely in their inherent physicochemical properties (see **Table 2** and **Section 2.2**), there are no uniform or standard methods of lubricant infusion and drainage. Some useful criteria to improve reproducibility in the field include consistency in the infusion/depletion processes and the characterisation of lubricant quantity.

Fig. 4 details some common methods of infusing lubricant and controlling its thickness through controlled depletion. **Table 3** and **Table 4** detail how surface and wettability properties change before and after infusion and depletion, respectively. As seen from these Tables, the range of methods used to infuse and drain lubricants are almost as varied as the choice of lubricant itself. For infusion, solution immersion[135, 163, 167, 301] and for depletion, gravimetric draining for specific times[73, 77, 133, 135, 154, 167, 303, 304] are the most popular choice (**Fig. 4A)i) Fig. 4B)i)**). Other methods to infuse lubricant and control its initial thickness include drop-casting,[171, 214] spin-coating, [64, 70, 75, 166] compressed air drying[61, 62, 214, 305]. However, these methods are relatively uncontrolled, particularly for lubricants that are volatile (**Table 4)**. In contrast, dip-coating is more reliable in preparing reproducible lubricant thickness due to greater control over coating parameters.

3D LIS are infused by immersion, with the substrate being submerged in the lubricant for an extended period (typically over 24h) to allow swelling to occur. In this case, the amount of lubricant in the overlayer is determined by several factors, including how the substrate is removed from the lubricant and how quickly the lubricant is excreted from the bulk.[38] As a result, characterisation of the lubricant present is integral to understanding the performance of these surfaces.

Table 3 - Methods commonly used for lubricant infusion. Contact angle measurements are made with water unless otherwise stated. Contact angle hysteresis (CAH) and roll-off angle measurements are distinguished using the superscript a and b, resepctively. The results listed in the table refer to the work listed in the first column; the references in the last column are other studies using the same method.

Method	CAH/Roll-off Angle (°)		Lubricant Quantification	Other Effects Tested	Also used in ref
	Before Infusion	After Infusion			
Solution Immersion[163]	24 ± 3°[a]	19 - 36°[a]	N	Ice adhesion	135, 167, 301
Spin-Coating[42]	14 - 30°[a]	<10°[a]	Y[d]	Ice adhesion	64, 70, 75, 98, 159, 166, 222, 227
Dip-Coating[16]	90°[b,c]	0.6 ± 0.2°[b,c]	Y[e]	Platelet adhesion/blood clotting time	133, 138, 143, 302
Solvent Exchange[62]	56.4 ± 1.4°[a] 90°[b]	1.4 ± 0.2°[a] 2-3°[b]	N	Corrosion resistance	61
Drop-cast[171]	90°[b]	2 ± 1°[b]	N	Anti-adhesion of various fluids	214
Vacuum-Suction[154]	>90°[b]	8 ± 1°[b]	N	Drag reduction	-
Electrospray[94]	N/A	4.4 ± 2.8°[a]	Y[e,f]	Ice adhesion	-

[a] contact angle hysteresis (CAH), [b] roll-off angle, [c] human whole blood, [d] SEM, [e] weight difference, [f] confocal microscopy

Other unique methods have been employed to infuse samples that cannot be infused using the simple methods already mentioned. For a sample with high aspect ratio pores that are not spontaneously filled by lubricant, a solvent exchange method was used. Here, low surface tension solvents that can penetrate the high ratio pores were sequentially filled with different liquids until the desired lubricant fills the cavities.[61, 62] Another method to fill pores from Lee *et al.* uses vacuum suction to applied negative pressure to extract air from cavities and allows the lubricant to fill the cavities.[154] For a sample that needed selective lubrication on the tops of microposts, Dong *et al.* use a robotic microdroplet deposition device to apply the lubricant layer.[87]

The resulting thickness of the lubricating layer in each method depends heavily on the system involved. For example, the thickness of the layer deposited in dip coating depends on both the removal speed and the viscosity of the liquid. The final film thickness is system-dependent and scales with employed preparation parameters. The maximum thickness achievable by all methods is much thicker than can be stabilised and the excess thickness will quickly deplete. Film thickness on the order of hundreds of nm to hundreds of µm is achievable with all methods, but in all cases determination of thickness and consistency is key.

Some studies do not explicitly mention the method used to infuse and/or deplete the surfaces with lubricant.[74, 176, 198] This is undesirable, as results cannot be reproduced by others. Reproducibly controlling the lubricant on the surface through a convenient, yet controllable method (e.g. dip coating or vertical draining to remove excess lubricant) combined with characterising the amount of lubricant on the surface (see **Section 5**) is key to enable comparison of results across studies.

4. Performance of LIS as a function of lubricant thickness and distribution

The performance of liquid-infused surfaces, including their omniphobic character, icephobicity, anti-bacterial, anti-corrosive, anti-fouling properties and drag reduction, is closely related to the volume and distribution of lubricant on the surface. This is similar to the failure of superhydrophobic surfaces due to plastron collapse,[306, 307] and even though the lubricant layer is more robust than an air layer, LIS are still most likely to fail due to loss of lubricant. Only a relatively small number of papers so far have specifically addressed the relationship between the performance of LIS and lubricant distribution, and the different mechanisms that lead to lubricant depletion.

The slippery properties (e.g. low roll-off angle and high interfacial slip length) of LIS likely depend on film thickness in a non-monotonic way. The limit at which the slippery properties start to degrade is likely to be of the order of tens of nm, and films thicker than this level are likely to be equally slippery, as long as they are homogeneous. Goodband *et al.* find little change in CAH as film thickness (estimated by change in mass) decreases from approx. 25 µm to 5 µm.[145] On a thick film (e.g. thicker than about 1 µm), the dynamic and static regimes of wetting are not affected by the exact lubricant film thickness.[130]

4.1. Performance of thin lubricant films in 1D LIS

In the absence of structural features, 1D LIS are unable to stabilise thick lubricant films. The films that remain are typically very thin (<5 nm) and stabilised via van der Waals or other intermolecular interaction.[33] The ability of very thin films to effectively lubricate is debated in 1D LIS research, with evidence pointing both to very low contact angle hysteresis and to more standard hydrophobic behaviour. The performance of 1D LIS is likely limited in time due to the low thickness of lubricant that can be stabilised compared to the structure of 2D LIS and the intrinsic reservoirs of 3D LIS. As there are relatively fewer publications concerning 1D LIS, it is difficult to make an accurate comparison of their performance.

Table 4 Methods commonly used for lubricant depletion. All contact angle measurements are made using water.

Method	CAH/Roll-off Angle (°)		Lubricant Quantification	Other Effect Tested	Also used in ref
	Before Infusion	After Infusion			
Gravimetric Draining[304]	46.5°[a]	2.5 ± 0.5 - 4.1 ± 0.9°[a]	N	Bacterial Growth	73, 77, 133, 135, 154, 167, 303
Spin Coat[133]	>90°[b, e], 10 ± 6°[b, f]	<5°[b, e], 3 ± 1°[b, f]	Y[c]	Bacterial Growth	81, 134, 155, 215
Blow-Dry with compressed air[214]	-	19 - 48°[a]	N	Ice adhesion	61, 62, 305
Water Spraying[94]	-	4.4 ± 2.8°[a]	Y[d]	Ice adhesion	-

[a] contact angle hysteresis, [b] roll-off angle, [c] fluorescence Microscopy, [d] weight Difference, [e] hydrophilic substrate, [f] hydrophobic substrate

Scarratt *et al.* found that the low amount of lubricant present in 1D LIS leads to distinct properties to those exhibited by surfaces with thicker lubricant layers. For example, a 2-nm thick silicone oil film stabilised by an octadecyltrichlorosilane (OTS) monolayer does not have strong drag-reducing properties,[130] which are only measured on thicker lubricant layers.[94, 308, 309] Scarratt *et al.* found that low roll-off angle on flat infused self-assembled monolayers disappears once the lubricant layer is thinner than about 20 nm.[130] On the other hand, others have found that 1D LIS exhibit many of the desirable properties associated with LIS. Zhang *et al*. show that a lubricant layer on a hydrophobic non-textured substrate exhibits low roll-off angles and delayed ice formation, but also that the layer thickness is drastically reduced after washing the sample with water.[20] Similarly, Eifert *et al.* show that lubricant is lost when a 1D LIS is held vertical, but that the surface is still slippery.[115] Wang *et al.* showed that silicone oil trapped using a molecular layer produces a slippery surface capable of repelling complex viscoelastic mixtures with impressive longevity that is extended with lubricant replenishment.[27]

Slippery Omniphobic Covalently Attached Liquid (SOCAL) surfaces are an attractive method to produce low adhesion

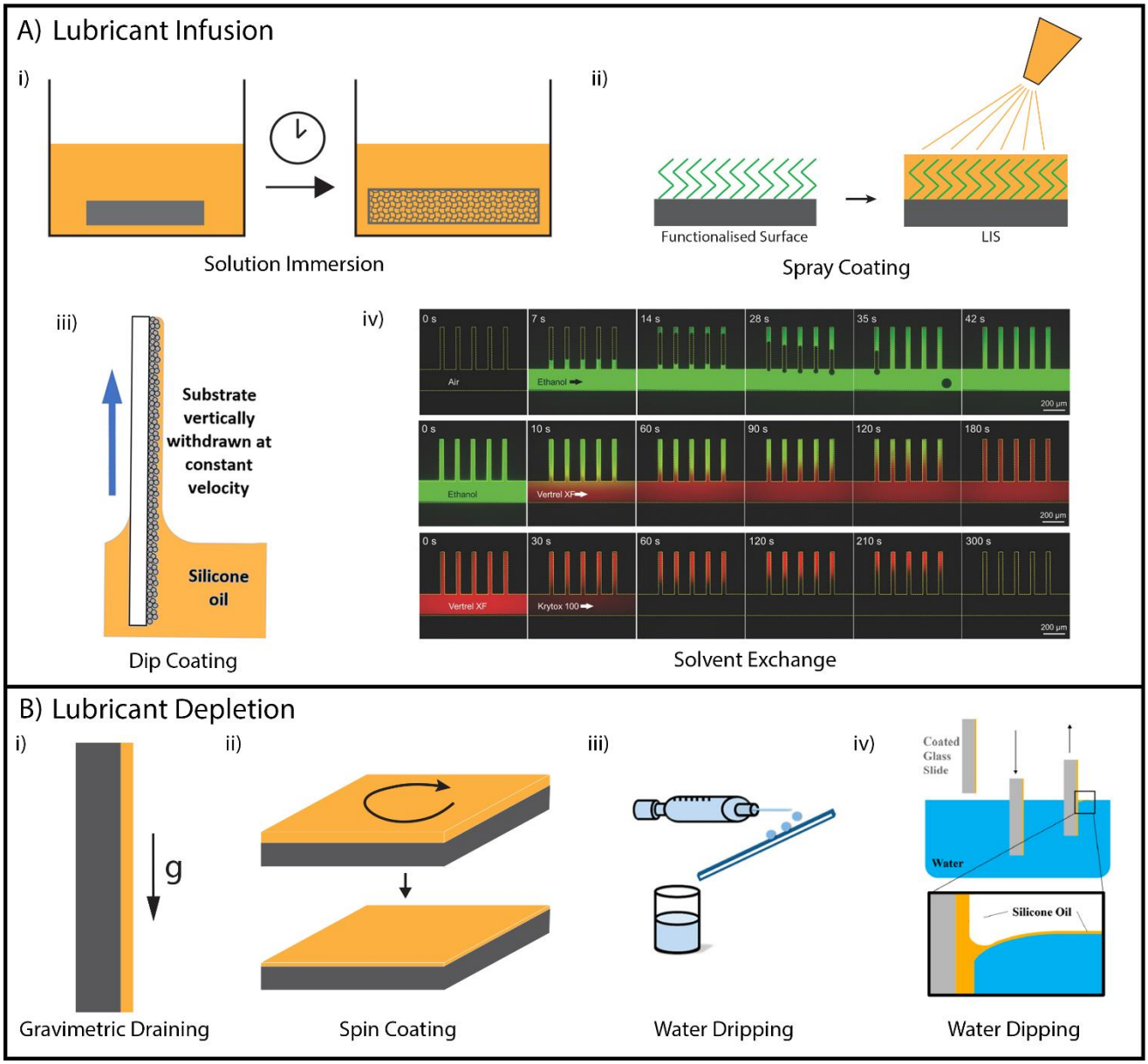

Fig. 4 – Common method of lubricant infusion (A) and depletion (B). A) i) Solution immersion is used for 3D LIS where the entire substrate is submerged in the lubricant so that the lubricant can diffuse into the substrate. ii) In spray coating, the lubricant is sprayed directly onto the surface. Inspired by [27]. © 2019 Spring Nature. iii) Dip coating deposits a thin liquid film as the substrate is pulled out from a reservoir of lubricant and gives good control over film thickness. Adapted with permission from [143]. © 2019 Springer Nature. iv) Solvent exchange process for filling high aspect ratio pores that are difficult to fill directly with the lubricant. Reproduced with permission from [61]. © 2019 Springer Nature. B) i) Gravimetric draining is the simplest depletion method, allowing excess lubricant to drain away under gravity. ii) Spin coating partially removes lubricant due to rotation induced shear. iii) Water dripping removes lubricant in the form of cloaking and wetting ridge around each droplet. Adapted with permission from [20]. © 2018 American Chemical Society. iv) Dipping through an air/water interface removes lubricant due to shear at the interface. Adapted with permission from [38]. © 2018 AIP Publishing.

surfaces as they do not suffer from depletion in the same way as the other types of LIS. Their performance relative to surfaces with mobile lubricant layers is difficult to gauge, however, as the main property that has been assessed on SOCAL surfaces is contact angle hysteresis.[25, 115, 310, 311] Wu *et al.* looked at how silicone brush SOCAL surfaces perform in regards to biofouling and have found that they perform well compared to hydrophilic controls and that they are much more robust than SLIPS against abrasion from sand and water.[312]

4.2. Methods to accelerate lubricant depletion

The common pathways by which lubricant is lost from 2D and 3D LIS are via spreading to surrounding surfaces, capillary effects, shear-induced by the flow of air or other working fluids, drainage induced by gravity, and evaporation. Some of these mechanisms have been studied quantitatively, using conditions which mimic realistic operation conditions. Spin coating is often used to demonstrate the robustness of a surface towards depletion. [81, 133, 155, 215, 222, 313] However, spin-coating is not representative of the realistic depletion pathways that the surface would typically undergo during use, and does not induce the same degree of film depletion as other more aggressive methods. More effective tests of depletion involve dripping water droplets repeatedly on the surface (as oil is removed from the surface in the meniscus surrounding every drop, see **Fig. 4B(iii)**), [62, 94, 148, 164, 191] shearing with a jet of nitrogen gas (by aerodynamic stress[130] and evaporation),[72, 180] shearing with a water jet,[91, 152, 314, 315] or even more effective, dipping the surface repeatedly across a water-air interface (see **Fig. 4B(iv)**).[38, 91] Other tests have attempted to characterise the slippery properties of a surface through expected use cases such as coming into contact with an unlubricated material,[44] icing/deicing cycles,[160] or in simulated underwater usage[55, 133, 190, 303]. Comparison of different accelerated depletion methods is difficult as there is no standard metric to measure the performance of LIS. Most commonly, slippery properties are assessed through contact angle hysteresis or roll-off angle, or the performance is assessed in a given application such as through bacterial or ice adhesion tests. **Table 4** details how wettability changes for LIS undergoing different accelerated depletion techniques.

4.3. Lubricant depletion induced by flow or shear

LIS are often tested in flow situations, as they offer potential for drag reduction in both laminar[102, 302, 316] and turbulent[317, 318] flows. However, when exposed to high flow rates, LIS become depleted due to shear-induced drainage.[143, 319, 320] The Stone group investigated the effect of viscosity ratio (the ratio of the viscosity of the working liquid over that of the infused liquid) on lubricant retention within streamwise grooves infused with lubricant and exposed to longitudinal flow within microfluidic devices.[321, 322] They found that a higher pressure gradient results in lower lubricant retention. Also, for a given shear stress, less viscous lubricants achieve higher retention because shear stress at the fluid-fluid interface decreases when the viscosity ratio increases. However, large viscosity ratios can cause instability at the liquid/liquid interface, which also triggers the failure of LIS.[323] The same group found that shear-induced drainage of the lubricant could be prevented by imposing a pattern of surface chemistry preferentially wetted by the working liquid rather than the lubricant on the substrate. By interrupting the continuity of the infused lubricant, these patterns prevent the lubricant from draining from the infused roughness.[320] In agreement with this observation, we have found that infused wrinkled Teflon surfaces are particularly effective at retaining lubricant, because the space between the wrinkles (feature width of the order of 100 nm) is not interconnected, and the gaps between wrinkles are of the order of a few micrometres.[324]

An area that requires further work is the study of the geometric surface parameters that enable most effective fluid retention under flow; limited work has been published both in regular and randomly patterned surfaces. [26, 36, 315] Numerical simulations suggest that there are multiple failure modes of LIS under flow. In a simple geometry of an infused groove, if the groove is deep enough, the lubricant meniscus will de-pin from the front of the groove leading to failure. For a shallow groove, the meniscus will contact the bottom.[325]

4.4. Methods of lubricant replenishment

To extend the lifetime of a surface past failure due to depletion, a few publications include the ability for the lubricant to be replenished from an external source. 3D LIS have the advantage that they store lubricant in their bulk and so self-replenish when their lubricious overlayer is removed.[38, 120, 139, 165, 232] The lubricant is infused into the matrix by diffusion,[38] and therefore can diffuse back to the surface. As a chemical gradient drives diffusion, the ability of 3D LIS to replenish their overlayer will diminish as more and more lubricant is removed and they too will need replenishment from some external source. Howell *et al*. achieved this through biomimicry of the vascularisation of leaves to embed a fractal system of channels in their iPDMS surface, allowing new lubricant to be pumped throughout the surface.[126] Other methods draw inspiration from subdermal glands and incorporate cavities into the material which fill with lubricant and provide a reservoir to replenish the overlayer.[45, 124, 136, 236]

For 1D and 2D LIS, replenishment is more urgent as the volume of lubricant on the surface is limited. Here, relubrication is more challenging as new lubricant must be introduced from above the surface. Baumli *et al*. introduce lubricant onto a pillared surface by flowing an oil-in-water emulsion across the surface.[146] They found that this filling is very robust, occurring for a range of velocities, lubricant concentrations, lubricant viscosities and surface chemistries. This presents a method that can effectively replenish LIS employed in an application under flow, in the interior of a pipe, for example. Wang *et al.* successfully replenish lubricant for a low-water usage toilet based in 1D LIS by simply spraying more silicone oil on the surface or by mixing silicone oil into the flushing liquid where it preferentially wets the surface.[27]

Another approach is to design the surface so that it is only slippery when it needs to be. Wu *et al.* achieve this by incorporating iron oxide nanoparticles into a lubricant that is solid at room temperature.[172] Irradiation of the surface with

infrared light heats the lubricant above its melting point and allows for the removal of contaminants and for the lubricant to flow back into any damaged areas. Chen *et al.* use joule heating to liquefy paraffin wax and create a switchable slippery surface.[235] Ye *et al.* achieve a similar effect using a 3D LIS with an ionic liquid lubricant that can only flow above its melting temperature, which is close to operating temperature.[43]

5. Characterisation of lubricant thickness and distribution

Key to the rational development of LIS is the characterisation of the lubricant distribution on the macro-, micro- and nanoscale, including dynamic effects. Essential questions to be answered include: how much lubricant is trapped on the surface at time zero and as the lubricant depletes from the surface? How homogenous is the layer thickness during ageing? How do droplets interact with the surface at different stages of depletion?

There are numerous challenges associated with the analysis of the lubricant layer. These layers are necessarily thin, making the volumes of lubricant present very small. Simple optical observation can help with the detection of the lubricant loss in the case of transparent 2D LIS (their roughness means they are only transparent when lubricated), the loss of transparency can be qualitatively correlated with a loss of infused layer.[35, 67, 69, 106, 168, 193, 196] For more detailed analysis in a broader variety of surfaces, more sensitive and general characterisation techniques are required.

Techniques reported for characterising lubricant layers fit into two broad categories: indirect and direct techniques. Indirect techniques rely on the measurement of the total lubricant present, while direct techniques attempt to spatially resolve lubricant thickness to understand how surface structure or interaction with droplets influence layer thickness. Techniques reported in the literature are summarised in **Table 5**.

5.1 Indirect methods

Indirect techniques measure the amount of lubricant on a surface with no spatial information on lubricant distribution. The most common of these is to measure the mass change of a test substrate before and after infusion or depletion.[27, 36, 67, 78, 109, 134, 145, 170] The balance used for the measurement and the size of the sample limits the resolution of this technique which is problematic for depleted lubricant films. For example, a liquid film of thickness 1 μm with density 2 g mL^{-1} (the highest density in **Table 2**) has a mass of 0.2 mg cm^{-2}. Mass changes of this order approach the limit of typical analytical laboratory balances.

A second approach uses fluorescence or UV spectroscopy to measure the volume of lubricant present on the surface with the scope to have much higher sensitivity than mass change.[133, 226] Ware *et al.* added the fluorophore Nile Red to silicone oil before infusion. After infusion and depletion steps, the fluorescent lubricant was extracted from the surface and its volume calculated through a volume/fluorescence intensity calibration curve. With this method, the authors were able to find that as little as 0.2 μL cm^{-2} of silicone oil gave effective anti-bacterial properties (76% inhibition) to wrinkled liquid-infused surfaces.[133] Fluorescently tagged lubricant has also been used

Table 5. Comparison of techniques currently used to characterise liquid layer thickness on LIS.

Technique	Lateral Resolution	Vertical Resolution	Temporal Resolution[a]	Possible substrates	Used in References
Indirect					
Mass change	-	-	-	Any	36, 67, 78, 109, 124, 134, 145, 170, 175, 215
Fluorescence/UV Spectroscopy	-	-	-	Any	133, 186, 226
Direct					
Laser scanning confocal microscopy	500 nm[b]	200 nm	Seconds	Transparent	37, 44, 47, 91, 124, 159, 176, 223, 252, 326-329
Scanning electron microscopy	10 nm	10 nm	Minutes	Any	37, 83, 87, 111, 113, 181, 212, 223, 226, 232, 330-332
Ellipsometry	1 mm	< 1 nm	Minutes	Flat	20, 148, 311
Interference microscopy	500 nm[b]	< 1 nm	Seconds	Any	59, 64, 333
Reflection interference contrast microscopy	500 nm[b]	10-30 nm	Milliseconds	Transparent	32, 59, 80, 86, 334
AFM Force mapping	< 10 nm	< 1 nm	Minutes	Any	33, 132

[a] timescales reported should only be interpreted as order of magnitude. Scan times for all techniques vary depending on scan size, resolution, sample etc., [b] based on the diffraction limit

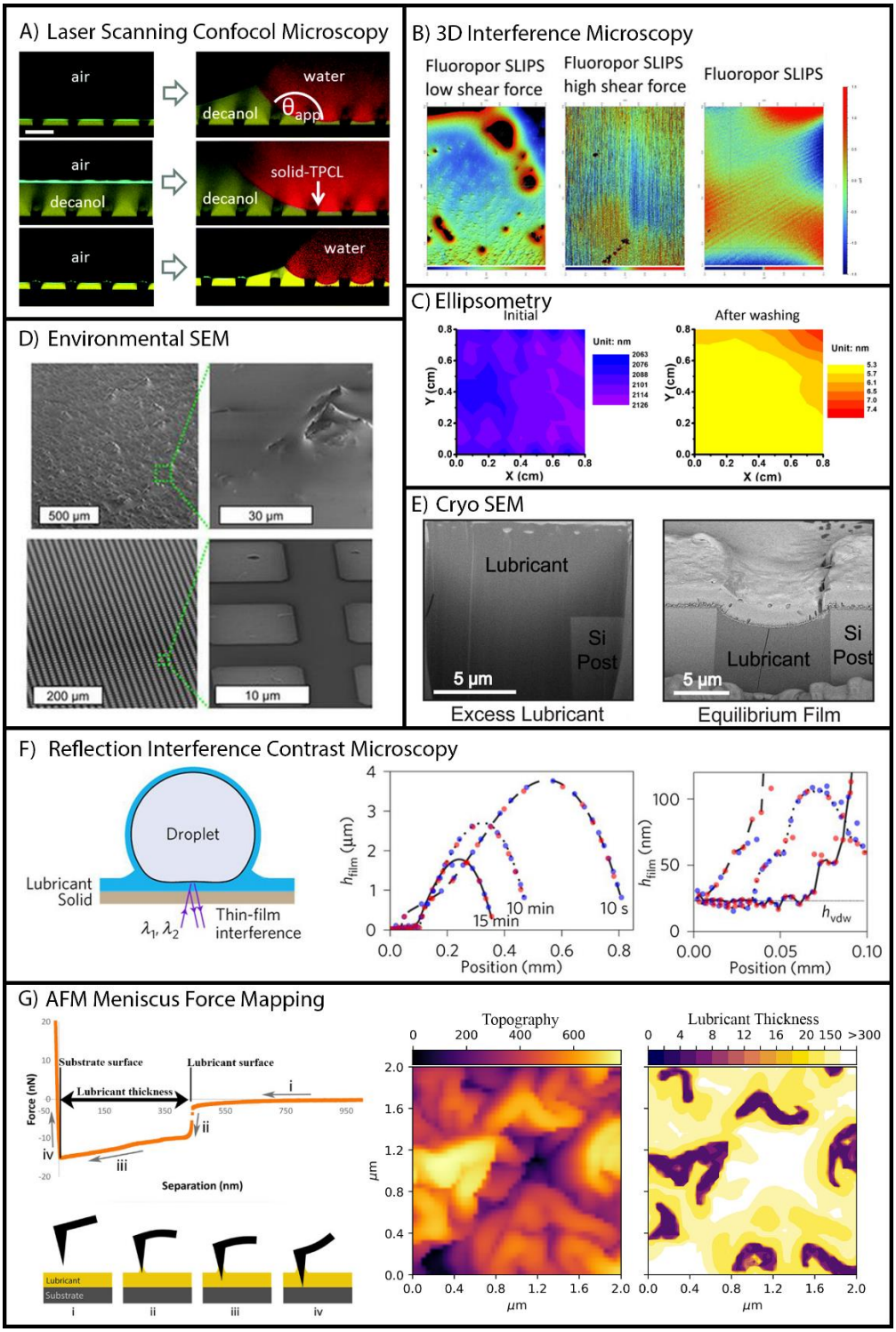

Fig. 5 – Direct lubricant characterisations methods. A) Laser scanning confocal microscopy allows for imaging the lubricant and droplets in 3D. The lubricant and water are dyed yellow and red respectively. Scale bar 40 µm. Adapted from [176] under Creative Commons 3.0. B) 3D Interference microscopy shows the structure of the lubricant surface, revealing the underlying structure when the lubricant depletes. Adapted with permission from [333]. © 2019 American Chemical Society. C) Ellipsometry provides exceptional precision in lubricant thickness but has limited lateral resolution. Adapted with permission from [20]. © 2018 American Chemical Society. D) Environmental SEM allows for the direct imaging of lubricant on the surface at high resolutions. Adapted from [113] under Creative Commons 3.0. E) Cryo SEM allows for direct imaging of cross-sections of LIS. © 2019 American Chemical Society. Adapted with permission from [212]. F) Reflection interference contrast microscopy allows for precise measurement of lubricant films under and around droplets with short collection times. Adapted with permission from [80]. © 2017 Nature Springer. G) AFM meniscus force measurements allow for exceptional lateral resolution and nanoscale precision in lubricant thickness. Adapted with permission from [33]. © 2018 American Chemical Society.

to estimate depletion by optical observation of fluorescence intensity after depleting the surface under shear.[186] Wu *et al.* monitored lubricant loss in a similar way but directly measured concentration using UV spectroscopy.[226]

Both these approaches give a reasonable estimate of the volume of oil infused into the surface and can give an estimate into thickness,[134] assuming a flat sample. These techniques, however, can overestimate the amount of lubricant as the lubricant may spread onto the back or sides of the sample and contribute to the volume measurement.

5.2. Direct methods

Direct techniques map or measure the thickness of oil on the surface to provide much greater detail than indirect techniques. One of the most commonly used methods is laser scanning confocal microscopy.[37, 44, 47, 91, 124, 159, 176, 195, 223, 252, 326-330, 332] This technique allows 3D imaging of substrate, lubricant and liquid drops on the surface simultaneously, and over time. In confocal microscopy, fluorescently dyed lubricant and working liquids are mapped in three dimensions, giving a stack of images that can be sliced arbitrarily.[335] For lubricated surfaces, the lubricant and liquid drops on the surface can be tagged with different dyes, allowing imaging of both, see **Fig. 5A**. Although perfluorinated fluids are difficult to fluorescently tag owing to their unique chemistry, Howell *et al.* produce fluorescent nanoparticles that partition into the perfluorinated phase to image perfluorinated lubricants.[91] Due to the slow collection times, of the order of seconds to minutes per frame, this technique is useful for equilibrium systems or slow-paced dynamic processes. For example, it has been used to image the condensation of a water drop on a lubricated surface.[223] There are a few drawbacks to using laser scanning confocal microscopy. To effectively image the lubricating layer, it is best to use the microscope in an inverted geometry, restricting analysis to transparent substrates. Films of thickness below 1 µm can be detected but not quantified. As the technique is based on visible light, interference at boundaries can occur, and the resolution of the technique is diffraction-limited, giving a maximum lateral resolution of about 500 nm.[336]

Other light-based techniques used include ellipsometry,[20, 148, 311] and interferometric techniques.[59, 64, 80, 333] Keller *et al.* used a 3D optical profiler (based on white light interference) to image the surface of the lubricant layer, revealing depletion when the underlying surface structure begins to protrude,[64, 333] see **Fig. 5B**. This technique provides excellent precision in height measurements but limited lateral resolution and cannot quantify lubricant thickness. Ellipsometry was used to map the thickness of lubricant on a flat lubricated surface, see **Fig. 5C**.[20] This technique gives very precise value of thickness (with error below 1 nm), but is limited in the *xy*-resolution by the spot size of the ellipsometer (approx. 1 mm on most instruments and down to approx. 10 µm on instruments with mapping capabilities) and is only suited to flat substrates. Interference microscopy was used to map the lubricant thickness on a porous surface, showing areas where lubricant had dewetted.[64] Daniel *et al.* used reflective interferometric contrast microscopy (RICM), to capture a lubricant film thickness through a transparent substrate underneath a droplet, see **Fig. 5F**.[80] This technique uses the interference of monochromatic light as it reflects off the boundaries of an infused layer to measure the thickness of the lubricant with vertical resolution of 10-30 nm.[337] Daniel *et al.* also used white light interference (similar to the 3D optical profiler mentioned above) to measure micrometric film thickness as RICM tends to underestimate film thickness for thicker films. As all the techniques mentioned in this paragraph are based on light, their lateral resolution is diffraction-limited.

Another often-employed direct measurement technique is scanning electron microscopy (SEM).[37, 83, 87, 112, 113, 172, 181, 182, 212, 226, 232, 330] Environmental scanning electron microscopy (ESEM) allows for higher chamber pressures, and so allows imaging of liquid systems including water.[338] This technique has been used to image lubricant in both randomly rough substrates and a regular array of micro-pillars,[37] see **Fig. 5D.** This technique provides qualitative images of lubricant distribution but cannot measure lubricant thickness. On the other hand, cryo-SEM allows for direct imaging of a lubricant layer when used in conjunction with focused ion beam (FIB) lithography to produce a cross-section of the surface showing the lubricant in a depleted state, see **Fig. 5E**.[112, 212] The surface can even be reconstructed in 3D using FIB tomography, but this process is slow and destructive.[112] One approach to investigating wetting at the nanoscale is to cure the liquid, making it solid, removing it from the surface and image it using SEM, although this has not been directly applied to LIS.[331]

Atomic force microscopy (AFM) meniscus force measurements allow quantification and mapping of the thickness of a thin liquid film on a surface. While AFM is routinely used to analyse surface topography and even the lubricant-water interface,[145] it can also provide quantitative data on lubricant thickness. Peppou-Chapman & Neto mapped the distribution of a lubricant film on a structured surface by performing AFM force maps over the infused substrate. When the AFM tip contacts the top of the liquid layer, a meniscus forms on the tip and draws it down, and this point signals the top of the layer. Hard contact with the substrate reveals the bottom of the layer and allows for the calculation of layer thickness, see **Fig. 5G**.[33] Mapping these forces across the surface builds a 3D map of not only lubricant thickness, but also the underlying substrate. This technique's resolution is only limited by the radius of the AFM tip used, giving a spatial resolution of less than 10 nm, with sub-nanometre resolution in thickness. Given the small size of the topographical features that typically hold lubricant in LIS, this technique reveals local lubricant distribution configuration at different stages of depletion, the local curvature of the lubricant interface and the stability and longevity of LIS. For example, Peppou-Chapman & Neto showed that excess lubricant is not held tightly and can easily flow away under external forces, with only the lubricant held by capillary forces remaining.[33, 132] The

slow collection time of AFM force curves makes it best suited to equilibrium measurements or slow processes.

6. Interaction of lubricant layer with droplets

The unique way in which water droplets interact with the lubricant layer on LIS is a vibrant area of study. The presence of the wetting ridge and cloaking layer fundamentally change how a droplet interacts with the surface, and the lubricant layer drastically reduces the friction a droplet feels on the surface. Both of these lead to an array of ways to manipulate droplets on LIS both spontaneously and with external driving forces.

6.1. The wetting ridge

The wetting ridge is a meniscus of lubricant drawn up around the base of the droplet through capillary action. The formation of this wetting ridge is unavoidable, and its size is a function of the amount of lubricant present on the surface, the length of time a droplet has been on the surface, and the velocity of the droplet.[59] Measuring the true contact angle of a droplet on a LIS is non-trivial as the wetting ridge hides the contact line and distorts the base of the droplet. Reported contact angles are generally apparent contact angles, calculated as the intersection of the solution to the Young-Laplace equation for the top of the droplet and a baseline defined by the top of the substrate. The size of the wetting ridge influences the actual contact angle of the droplet.[243, 339]

The wetting ridge is a region of negative Laplace pressure owing to its negative curvature and so draws more lubricant into it over time.[59] The equilibrium height of the wetting ridge is determined by the balance of Laplace pressure and hydrostatic pressure, and the shape is a modified Bessel function of the second kind, approximated by $z = exp(-r/\ell_c)$ where r is the radial position and ℓ_c the capillary length, see **Fig. 6A**.[176] The equilibrium size of the wetting ridge for a static droplet is related to the amount of lubricant on the surface with a relatively long timescale to come to equilibrium, see **Fig. 6B**.[243] For a moving droplet, lubricant is also drawn into the wetting ridge and deposited behind it, with the thickness entrained varying with velocity, analogous to the Landau-Levich-Derjaguin (LLD) problem.[59] This leads to depletion as lubricant is lost with each drop that rolls off the surface.[59, 340] Somewhat paradoxically, more lubricant is lost with slower-moving droplets as these entrain more lubricant in their wetting ridge.[59] Although droplets moving on LIS oleoplane,[80] energy is lost through viscous dissipation in the wetting ridge,[128] causing droplet motion to be dependent on the size of the droplet.[65]

6.2. The cloaking layer

Depending on the combination of lubricant/droplet, the lubricant can spontaneously spread over the droplet in a thin cloaking layer ($S_{ld} > 0$). The thickness of this layer is of the order of nm with estimates of around 20 nm for a PFPE lubricant on a water droplet found by balancing the Laplace pressure in the cloaking layer with the disjoining pressure.[176] Direct observation of the cloaking layer using white light interference shows that the layer is not homogenous across the surface area of the droplet with thickness between 10-500 nm, see **Fig. 6C**.[59] The presence of the cloaking layer has also been confirmed by confocal microscopy,[176] but its thickness cannot be quantified using this technique. The volume of lubricant in the cloaking layer is much lower than is contained in the wetting ridge and, as a result, the cloaking layer does not contribute substantially to the depletion of lubricant from the surface.[59]

6.3. Droplet friction

LIS are often referred to as *slippery* owing to their low adhesion and very low droplet roll-off angles. Quantification of the friction force generated by droplets as they move on these surfaces reveals that LIS are indeed distinct from solid surfaces (including superhydrophobic surfaces) in the way that droplets move across them. For a drop moving on a solid surface, energy is dissipated through viscous dissipation in the droplet itself and pinning/depinning events at the contact line.[326] On LIS, contact line pinning is absent as there is no solid/liquid/gas contact line, and hence, the friction is lower as a droplet moves across the surface.

There are two ways to measure the force required to move a droplet on a surface, and by extension, the friction generated between the two. The first is to measure the terminal velocity of a droplet rolling off the surface at a given tilt angle,[128, 334] and the second is to directly measure the force required to move the droplet using a calibrated cantilever.[59, 80, 334] (**Fig. 6D**). The latter gives insight into the mechanism of how droplets start moving in addition to giving the equilibrium force on the droplet during motion.

Keiser *et al.* utilised the tilting technique to analyse the relationship between terminal velocity, V, and tilt angle, α, as a function of relative viscosity on 2D LIS.[128] The relative viscosity between the droplet and lubricant influences the velocity of the shed droplet, with the more viscous of the two determining where energy is dissipated. If the droplet is much more viscous than the lubricant (or vice versa), the friction is linear in speed (follows Stokes Law) with $V \sim sin(\alpha)$. This is analogous to a solid surface with almost all the dissipation occurring within the droplet (or the droplet cannot deform the lubricant in the case of the lubricant being much more viscous than the droplet).[128] When the lubricant is more viscous than the droplet (but not much more viscous), the scaling depends on the tilt angle: $V \sim sin(\alpha)^{3/2}$ for small α, and $V \sim sin(\alpha)^3$ for large α.[128] In this case, dissipation occurs mostly in the lubricant in the wetting ridge and underneath the droplet, but also in the droplet itself.[128, 341] Directly measuring the force required to move a droplet allows for an investigation of the non-equilibrium behaviour of a droplet before it reaches its terminal velocity. This reveals that when droplets start moving on 2D LIS, there is initially higher force before they reach a steady state.[334] This higher force is reminiscent of static friction described in classical mechanics, but once the droplet is moving the friction force $F \sim Ca^{2/3}$ (where Ca is the capillary number) is lower than this initial barrier.[334] The equilibrium force (at terminal velocity) for a 2D LIS is much lower than that on a superhydrophobic surface or a SOCAL surface (1D LIS),[334] due to the absence of energy dissipation at the contact line.[80]

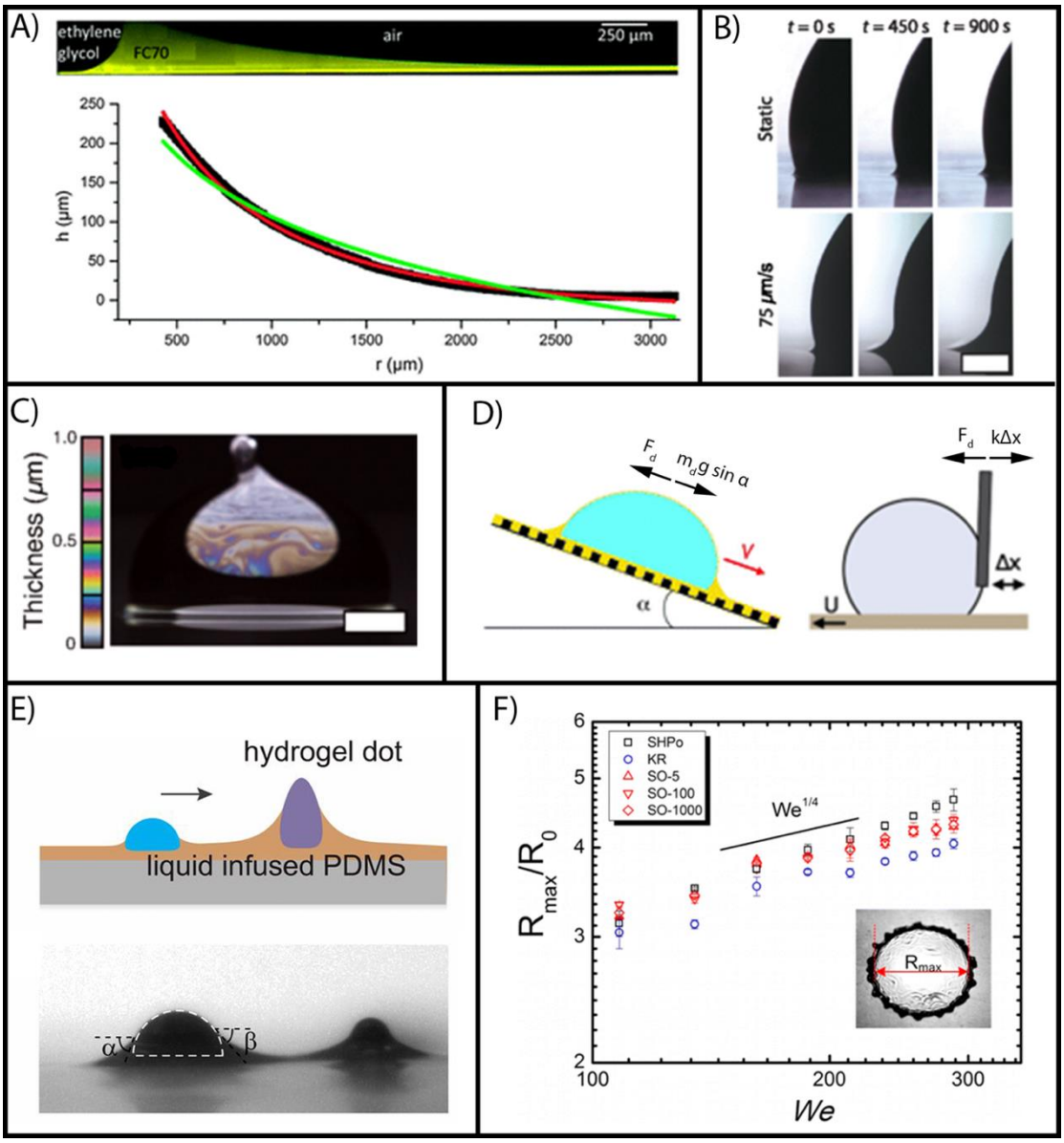

Fig. 6 – A) Direct observation of the shape of the wetting ridge (black line) using confocal microscopy with fits. Red: catenoid; green: nonoid. Reproduced from [176] under Creative Commons 3.0. B) The size of the wetting ridge increases in time when the drop is static or in motion. Scale bar = 0.5 mm) Adapted from [59] under Creative Commons 4.0. C) Visualisation of the cloaking layer using white light interferometry on a moving droplet. The thickness scale on the left is calculated and should be used only as a guide. Scale bar = 1 mm. Adapted from [59] under Creative Commons 4.0. D) Different ways to measure the force required to move a droplet: by measuring the terminal velocity where droplet friction F_d balances the driving force $m_d g$ sin α (where m_d is the mass of the droplet); or by measuring the deflection of a calibrated cantilever as the substrate moves underneath the droplet. Adapted from [128] with permission of the Royal Society of Chemistry and [334] with permission © 2018 American Physical Society. E) The wetting ridge can cause directional pumping of drops due to unequal capillary force created by an adjacent wetting ridge. Adapted from [127]. F) The ratio of the maximal spread of an impacting droplet to the original size of the droplet generally scales with $We^{1/4}$. There are some exceptions, such as when the droplet is more viscous than the lubricant. Reproduced with permission from [60] © 2014 American Chemical Society.

The friction felt by a droplet as it moves across a LIS always scales with $F \sim V^{2/3}$ even though there are multiple sources of friction in the wetting ridge and underneath the droplet.[342] As these sources all scale with $F \sim Ca^{2/3}$, the overall friction scales with $F \sim V^{2/3}$. This relationship is robust, and data obtained from 2D LIS with different pillar heights and collected using both techniques mentioned above collapsing onto a single curve.[342]

6.4. Droplet motion

As the friction felt by the droplet dominates its motion, the same underlying forces are important: contact line pinning and viscous dissipation. For droplets on solid surfaces, contact line pinning governs the motion of the droplet. For LIS, there is no contact line pinning, meaning viscous dissipation dominates droplet motion.

As a result of the high mobility of droplets on LIS, very weak driving forces are needed to move droplets. Stimuli-responsive LIS were recently reviewed,[12] and here only a few examples are highlighted. A thermal gradient as small as 2 K mm^{-1} can induce thermocapillary motion for a droplet, moving it towards the cooler temperature.[343] Surface acoustic waves allow for guided

droplet transport with no degradation of droplet mobility through extended use of the technique.[140] A vibrating surface can propel a droplet either up or down an inclined surface with the direction depending on the oscillation rate.[197] Chemically inhomogeneous surfaces allow for liquid-liquid patterning where regions of high surface energy are preferentially wet by a chemically compatible liquid and all other areas remain covered in lubricant.[97] For example, an ethanol droplet deposits itself on hydrophilic regions as it rolls across a LIS, leaving a predefined pattern of micro drops.[56, 97] Droplets rolling under gravity can also be directed along pre-defined high-surface energy paths.[192] Areas of differing wettability allow different lubricants to be spatially separated so that highly mobile droplets can be guided along predefined tracks.[105] A deformable LIS enables guided droplet transport by creating a moveable depression into which the droplet rolls.[89] Shaping LIS so that a droplet is not round causes droplet motion as it moves to remove tension in its contact line.[137, 138]

The interaction of the adjacent wetting ridges can spontaneously manipulate droplets. When two wetting ridges begin to overlap, they 'zip-up', drawing adjacent droplets together.[86, 127, 344] The driving force behind this is an uneven capillary force from the wetting ridge, pulling the droplet towards the side with higher lubricant level.[86, 127] The droplets do not immediately coalesce due to the cloaking layer, and a unique interface between the two droplets is formed, where they are separated by a thin layer of oil that can be spontaneously replaced by lipids, forming a stable bilayer.[344] The lifetime of the thin oil film can be up to hours, with eventual drainage of the oil leading to coalescence.[344] The spontaneous movement of droplets due to wetting ridge interaction can also be exploited for spontaneous guided droplet transport by placing a hydrophilic bump under the lubricant. This forms a large wetting ridge type structure, drawing any nearby droplets to the hydrophilic bump, see **Fig. 6E**.[127, 149] This phenomenon also increases the efficiency of LIS in condensation applications as it causes microdroplets to spontaneous move towards and coalesces with larger droplets, allowing faster droplet shedding.[86] Interaction of wetting ridges on adjacent grooves causes the droplets to self-align in long chains perpendicular to the grooves.[330] It should be noted that all these phenomena require a thick lubricating layer.

6.5 Droplet impact

Droplet impact studies on LIS were recently reviewed,[11] so only some key points are summarised here, paying particular attention to the similarities and differences between LIS and superhydrophobic surfaces.

Droplet impact is measured in terms of the non-dimensional Weber Number $We = \rho v^2 l/\sigma$, where ρ is the density of the fluid, v is the velocity, l is the characteristic length scale (usually droplet diameter), and σ is the interfacial tension. Generally, droplet impact is characterised by the ratio of the maximal spread diameter (R) to the initial droplet diameter before impact (R_0), R/R_0. When a droplet impacts on a non-wetting surface, the maximal spreading scales with $We^{1/4}$, see **Fig. 6F**.[345] This is mostly true with LIS, with several reports supporting this scaling.[60, 64, 150, 158] Droplet impacts do not always follow this scaling, however, with droplets with a higher viscosity than water showing a scaling closer to $We^{1/5}$.[150, 158]

LIS and superhydrophobic surfaces exhibit similar properties, but the presence of the lubricant layer causes several differences in how droplets impact. The most notable of these is that LIS have higher static adhesion, so droplets generally do not bounce off the surface of LIS. The exception of this is for impacts with $We < 10$, where a thin air layer is trapped, and the surface exhibits superhydrophobic-like bouncing.[90] In this case, the thickness of the lubricant layer is essential, with critical thickness for bouncing $h_c \sim (\mu_0 We^{-2})^{1/3}$ where μ_0 is the viscosity of the lubricant.[90] Numerical studies have calculated the height and dynamics of this air layer as well as how the air layer deforms the lubricant layer.[346] When a droplet reaches its maximal spread, there is a delay before the droplet retracts, a phenomenon unique to LIS and thought to be due to viscous losses at the contact line.[158] The thickness of the lubricant layer does not influence droplets dynamics,[64] although it is not clear how this changes at the depletion limit when the surfaces start to fail.

7. Conclusions and outlook

Liquid-infused surfaces are currently poised to impact several industries due to their outstanding anti-adhesive properties. LIS provide a vibrant platform to study wetting at complex interfaces, adaptive wetting and responsive systems, with highly sophisticated fundamental studies already illustrating this. At the same time, LIS demonstrate a large potential for widespread application, as their performance and stability are undeniably superior to superhydrophobic surfaces with regards to repelling contaminated aqueous solutions and low surface tension liquids. Our in-depth survey of the literature has shown that although LIS design includes different lubricant stabilisation mechanisms and a vast array of lubricants, the lubricant layer remains the most important feature.

As a result, correct lubricant choice is paramount to the successful production of LIS, but is no simple task with our survey of the literature showing that there are more than fifty different lubricants reported. Although there is no ideal lubricant for use in every application, most lubricants fall into two classes: silicone compounds and perfluorinated compounds. These are popular due to their chemical stability, their immiscibility with most liquids and their low surface tension. Choice of lubricant class and specific parameters depends on the specific application, and to aid this decision, we have provided an overview of key design principles for LIS, summarising key publications that provide a framework for rational lubricant choice. With these tools and sufficient knowledge of chemical and physical properties of a system, one can design a LIS to repel almost any fluid. As LIS find wider application, environmental and medical factors will increasingly influence lubricant choice with questions of environmental effects, health effects and consumer attitudes towards lubricants becoming more pressing. Regarding this, we recommend the investigation of naturally derived lubricants

with clear environmental degradation pathways such as plant oils, and investigation of binary/ternary lubricant systems and functional lubricants.

Analysis of the lubricant layer is challenging but is integral to a fundamental understanding of the complex wetting phenomena related to LIS. Given that most publications do not perform any analysis of the lubricant layer, this is a challenge for the field. To aid future researchers, we have given an overview of currently used methods to quantify lubricant distribution and examples of the data they provide. While no method is ideal for all situations, we recommend that researchers use multiple characterisation methods to allow for greater comparison between studies.

Our research and survey of the literature have clearly highlighted a need to quantify the performance of LIS over time and with use. Their performance is dependent on a lubricant film being stable, uniformly distributed and of a thickness sufficient to provide slippery properties. With the most likely failure mode for all LIS being depletion of lubricant, an understanding of the mechanisms and pathways involved is vitally important. Lubricant films of thickness of the order of 1 μm and above are effective to reduce adhesion in most applications. However, several depletion mechanisms act to deplete the lubricant layer upon use, namely removal when the surface crosses the air/water interface, flow-induced shear, gravity-induced drainage and, for the higher vapour pressure lubricant, evaporation. The thickness of lubricant then easily decreases to a few hundred nm and below, and the initial performance may deteriorate or be lost. Further development of methods to replenish lubricant *in situ* is desirable, with several methods already published. The chemical degradation of lubricant through extended exposure to foulants has not been explored in the literature. Although lubricants are generally chosen for their chemical stability and immiscibility, foulants may be enriched gradually and over time into the lubricant and degrade its performance.

Due to a lack of consistency in experimental techniques for simulating lubricant depletion and no standard techniques for testing performance, it is difficult to compare performance between reported LIS. This inconsistency extends to more than just testing sample longevity, also impacting the reporting of samples in their *as-prepared* state. Most infusion methods produce a large excess of non-stabilised lubricant that will quickly flow away under any depleting force and testing a sample in this state is not representative of its performance in an application. Instead, samples need to be depleted to a standard level before any testing to allow for meaningful comparison across platforms of LIS. Going forward, we recommend that sample preparation and any depletion tests are coupled with analysis of the distribution, or at the very least, the quantity of lubricant on the surface.

As research in LIS moves out of the lab and into applications, the focus must shift from simply the manufacture of slippery surfaces to fully optimised surfaces for a given purpose and to a deeper understanding of the physical wetting phenomena underlying their function. In the pursuit of creating fully optimised surfaces, research must shift to combining the favourable properties imparted by the lubricant layer with other functionalities in the substrate or lubricant to create multifunctional surfaces.

Conflicts of interest

The authors declare no conflicts of interest.

Acknowledgements

AW thanks The University of Sydney Nano Institute for support through their Grand Challenge. CN acknowledges funding by the Australian Research Council under the Future Fellowship scheme. SPC thanks the University of Sydney and The University of Sydney Nano Institute for funding through their mobility program. SPC and JKH acknowledge the Australian Government Research Training Program (RTP) Scholarship for support. JKH acknowledges The Heart Research Institute for support. Financial support provided by the Clive and Vera Ramaciotti Foundations Health Investment Grant and Vanguard Grant (103004) from the National Heart Foundation of Australia.

References

1 T. S. Wong, S. H. Kang, S. K. Tang, E. J. Smythe, B. D. Hatton, A. Grinthal and J. Aizenberg, *Nature*, 2011, **477**, 443-447.
2 A. Lafuma and D. Quéré *Europhys. Lett.*, 2011, **96**, 4.
3 I. Sotiri, J. C. Overton, A. Waterhouse and C. Howell, *Exp. Biol. Med.*, 2016, **241**, 909-918.
4 C. Howell, A. Grinthal, S. Sunny, M. Aizenberg and J. Aizenberg, *Adv. Mater.*, 2018, **30**, e1802724.
5 D. J. Preston, Z. Lu, Y. Song, Y. Zhao, K. L. Wilke, D. S. Antao, M. Louis and E. N. Wang, *Sci. Rep.*, 2018, **8**, 540.
6 M. J. Kreder, J. Alvarenga, P. Kim and J. Aizenberg, *Nat. Rev. Mater.*, 2016, **1**, 15.
7 M. Villegas, Y. Zhang, N. Abu Jarad, L. Soleymani and T. F. Didar, *ACS Nano*, 2019, **13**, 8517-8536.
8 S. S. Latthe, R. S. Sutar, A. K. Bhosale, S. Nagappan, C.-S. Ha, K. K. Sadasivuni, S. Liu and R. Xing, *Prog. Org. Coat.*, 2019, **137**, 105373.
9 G. Mackie, L. Gao, S. Yau, D. C. Leslie and A. Waterhouse, *Trends Biotechnol.*, 2019, **37**, 268-280.
10 X. Lou, Y. Huang, X. Yang, H. Zhu, L. Heng and F. Xia, *Adv. Funct. Mater.*, 2020, DOI: 10.1002/adfm.201901130, 1901130.
11 Y. Liu, X. Yan and Z. Wang, *Biosurf. Biotribol.*, 2019, **5**, 35-45.
12 X. Yang, Y. Huang, Y. Zhao, X. Zhang, J. Wang, E. E. Sann, K. H. Mon, X. Lou and F. Xia, *Front. Chem.*, 2019, **7**, 826.
13 Z. Ashrafi, L. Lucia and W. Krause, *ACS Appl. Mater. Interfaces*, 2019, **11**, 21275-21293.
14 S. Miguel, A. Hehn and F. Bourgaud, *J. Biotechnol.*, 2018, **265**, 109-115.
15 H. F. Bohn and W. Federle, *Proc. Natl. Acad. Sci. U.S.A.*, 2004, **101**, 14138-14143.
16 D. C. Leslie, A. Waterhouse, J. B. Berthet, T. M. Valentin, A. L. Watters, A. Jain, P. Kim, B. D. Hatton, A. Nedder, K. Donovan, E. H. Super, C. Howell, C. P. Johnson, T. L. Vu, D. E. Bolgen, S. Rifai, A. R. Hansen, M. Aizenberg, M. Super, J. Aizenberg and D. E. Ingber, *Nat. Biotechnol.*, 2014, **32**, 1134-1140.
17 M. Badv, I. H. Jaffer, J. I. Weitz and T. F. Didar, *Sci. Rep.*, 2017, **7**, 11639.
18 R. A. Janssen and G. D. Sorenson, *US Pat.,* US7041088B2, 1987.

19 M. Karakelle and R. J. Zdrahala, *European Pat.,* EP89102378A, 1988.
20 C. Zhang, Y. Xia, H. Zhang and N. S. Zacharia, *ACS Appl. Mater. Interfaces*, 2018, **10**, 5892-5901.
21 M. Tenjimbayashi, R. Togasawa, K. Manabe, T. Matsubayashi, T. Moriya, M. Komine and S. Shiratori, *Adv. Funct. Mater.*, 2016, **26**, 6693-6702.
22 R. Togasawa, M. Tenjimbayashi, T. Matsubayashi, T. Moriya, K. Manabe and S. Shiratori, *ACS Appl. Mater. Interfaces*, 2018, **10**, 4198-4205.
23 K. Manabe, M. Nakano, Y. Hibi and K. Miyake, *Adv. Mat. Interfaces*, 2020, DOI: 10.1002/admi.201901818, 1901818.
24 L. Wang and T. J. McCarthy, *Angew. Chem. Int. Ed.*, 2016, **55**, 244-248.
25 J. W. Krumpfer and T. J. McCarthy, *Faraday Discuss.*, 2010, **146**, 103-111.
26 S. Wooh and D. Vollmer, *Angew. Chem. Int. Ed.*, 2016, **55**, 6822-6824.
27 J. Wang, L. Wang, N. Sun, R. Tierney, H. Li, M. Corsetti, L. Williams, P. K. Wong and T.-S. Wong, *Nat. Sustain.*, 2019, **2**, 1097-1105.
28 X. Wang, Z. Wang, L. Heng and L. Jiang, *Adv. Funct. Mater.*, 2020, **30**, 1902686.
29 P. Liu, H. Zhang, W. He, H. Li, J. Jiang, M. Liu, H. Sun, M. He, J. Cui, L. Jiang and X. Yao, *ACS Nano*, 2017, **11**, 2248-2256.
30 J. Escorihuela and H. Zuilhof, *J. Am. Chem. Soc.*, 2017, **139**, 5870-5876.
31 Z. H. Wang and H. Zuilhof, *J. Mater. Chem. A*, 2016, **4**, 2408-2412.
32 D. Daniel, A. Y. T. Chia, L. C. H. Moh, R. Liu, X. Q. Koh, X. Zhang and N. Tomczak, *Commun. Phys.*, 2019, **2**, 105.
33 S. Peppou-Chapman and C. Neto, *ACS Appl. Mater. Interfaces*, 2018, **10**, 33669-33677.
34 R. Seemann, S. Herminghaus and K. Jacobs, *Phys. Rev. Lett.*, 2001, **86**, 5534-5537.
35 A. Owais, T. Smith-Palmer, A. Gentle and C. Neto, *Soft Matter*, 2018, **14**, 6627-6634.
36 P. Kim, M. J. Kreder, J. Alvarenga and J. Aizenberg, *Nano Lett.*, 2013, **13**, 1793-1799.
37 J. D. Smith, R. Dhiman, S. Anand, E. Reza-Garduno, R. E. Cohen, G. H. McKinley and K. K. Varanasi, *Soft Matter*, 2013, **9**, 1772-1780.
38 I. Sotiri, A. Tajik, Y. Lai, C. T. Zhang, Y. Kovalenko, C. R. Nemr, H. Ledoux, J. Alvarenga, E. Johnson, H. S. Patanwala, J. V. I. Timonen, Y. Hu, J. Aizenberg and C. Howell, *Biointerphases*, 2018, **13**, 06D401.
39 J. Lv, X. Yao, Y. Zheng, J. Wang and L. Jiang, *Adv. Mater.*, 2017, **29**, 1703032.
40 W. L. Hinze, I. Uemasu, F. Dai and J. M. Braun, *Curr. Opin. Colloid Interface Sci.*, 1996, **1**, 502-513.
41 P. Zhang, C. Zhao, T. Zhao, M. Liu and L. Jiang, *Adv. Sci.*, 2019, **6**, 1900996.
42 W. Cui and T. A. Pakkanen, *J. Colloid Interface Sci.*, 2019, **558**, 251-258.
43 L. Ye, F. Chen, J. Liu, A. Gao, G. Kircher, W. Liu, M. Kappl, S. Wegner, H.-J. Butt and W. Steffen, *Macromol. Rapid Commun.*, 2019, **40**, 1900395.
44 R. Mukherjee, M. Habibi, Z. T. Rashed, O. Berbert, X. Shi and J. B. Boreyko, *Sci. Rep.*, 2018, **8**, 11698.
45 T. Li, Y. Zhuo, V. Håkonsen, S. Rønneberg, J. He and Z. Zhang, *Coatings*, 2019, **9**, 602.
46 L. Wu, Z. Dong, H. Du, C. Li, N. X. Fang and Y. Song, *Research*, 2018, **2018**, 4795604.
47 S. Basu, B. M. Hanh, J. Q. Isaiah Chua, D. Daniel, M. H. Ismail, M. Marchioro, S. Amini, S. A. Rice and A. Miserez, *J. Colloid Interface Sci.*, 2020, **568**, 185-197.
48 C. Urata, G. J. Dunderdale, M. W. England and A. Hozumi, *J. Mater. Chem. A*, 2015, **3**, 12626-12630.
49 V. P. Bavaro, *European Pat.,* EP1951330A2, 2005.
50 S. Hattori, K. Kamdar and J. A. Hart, *European Pat.,* EP0380102A1, 1990.
51 J. G. Nawrocki and D. D. Jamiolkowski, *US Pat.,* US7041088B2, 2003.
52 I. Wright, Aerospace Applications for PFPE Lubricants, https://www.engineering.com/AdvancedManufacturing/ArticleID/14969/Aerospace-Applications-for-PFPE-Lubricants.aspx, (accessed 14/01, 2020).
53 G. H. Ban, J. Lee, C. H. Choi, Y. Li and S. Jun, *LWT-Food Sci. Technol.*, 2017, **84**, 359-363.
54 X. C. Chen, K. F. Ren, J. Wang, W. X. Lei and J. Ji, *ACS Appl. Mater. Interfaces*, 2017, **9**, 1959-1967.
55 K. Doll, E. Fadeeva, J. Schaeske, T. Ehmke, A. Winkel, A. Heisterkamp, B. N. Chichkov, M. Stiesch and N. S. Stumpp, *ACS Appl. Mater. Interfaces*, 2017, **9**, 9359-9368.
56 W.-P. Huang, X. Chen, M. Hu, D.-F. Hu, J. Wang, H.-Y. Li, K.-F. Ren and J. Ji, *Chem. Mater.*, 2019, **31**, 834-841.
57 Y. Jiao, X. Lv, Y. Zhang, C. Li, J. Li, H. Wu, Y. Xiao, S. Wu, Y. Hu, D. Wu and J. Chu, *Nanoscale*, 2019, **11**, 1370-1378.
58 P. Kim, T.-S. Wong, J. Alvarenga, M. J. Kreder, W. E. Adorno-Martinez and J. Aizenberg, *ACS Nano*, 2012, **6**, 6569-6577.
59 M. J. Kreder, D. Daniel, A. Tetreault, Z. L. Cao, B. Lemaire, J. V. I. Timonen and J. Aizenberg, *Phys. Rev. X*, 2018, **8**, 031053.
60 C. Lee, H. Kim and Y. Nam, *Langmuir*, 2014, **30**, 8400-8407.
61 J. Lee, S. Shin, Y. H. Jiang, C. Jeong, H. A. Stone and C. H. Choi, *Adv. Funct. Mater.*, 2017, **27**, 11.
62 J. Lee, S. Wooh and C.-H. Choi, *J. Colloid Interface Sci.*, 2020, **558**, 301-309.
63 Y. Lu, G. J. He, C. J. Carmalt and I. P. Parkin, *RSC Adv.*, 2016, **6**, 106491-106499.
64 M. Muschi, B. Brudieu, J. Teisseire and A. Sauret, *Soft Matter*, 2018, **14**, 1100-1107.
65 Q. N. Pham, S. Zhang, K. Montazeri and Y. Won, *Langmuir*, 2018, **34**, 14439-14447.
66 Y. J. Tuo, H. F. Zhang, W. P. Chen and X. W. Liu, *Appl. Surf. Sci.*, 2017, **423**, 365-374.
67 N. Vogel, R. A. Belisle, B. Hatton, T. S. Wong and J. Aizenberg, *Nat. Commun.*, 2013, **4**, 2167.
68 J. Wang, K. Kato, A. P. Blois and T. S. Wong, *ACS Appl. Mater. Interfaces*, 2016, **8**, 8265-8271.
69 Y. Wang, H. F. Zhang, X. W. Liu and Z. P. Zhou, *J. Mater. Chem. A*, 2016, **4**, 2524-2529.
70 P. B. Weisensee, Y. Wang, H. Qian, D. Schultz, W. P. King and N. Miljkovic, *Int. J. Heat Mass Transfer*, 2017, **109**, 187-199.
71 T. Xiang, M. Zhang, H. R. Sadig, Z. Li, M. Zhang, C. Dong, L. Yang, W. Chan and C. Li, *Chem. Eng. J.*, 2018, **345**, 147-155.
72 J. Zhang, L. Wu, B. Li, L. Li, S. Seeger and A. Wang, *Langmuir*, 2014, **30**, 14292-14299.
73 P. F. Zhang, H. W. Chen, L. W. Zhang, T. Ran and D. Y. Zhang, *Appl. Surf. Sci.*, 2015, **355**, 1083-1090.
74 D. Daniel, M. N. Mankin, R. A. Belisle, T.-S. Wong and J. Aizenberg, *Appl. Phys. Lett.*, 2013, **102**, 231603.
75 X. Huang, J. D. Chrisman and N. S. Zacharia, *ACS Macro Let.*, 2013, **2**, 826-829.
76 D. Seo, J. Lee, C. Lee and Y. Nam, *Sci. Rep.*, 2016, **6**, 24276.
77 P. Wang, D. Zhang, Z. Lu and S. M. Sun, *ACS Appl. Mater. Interfaces*, 2016, **8**, 1120-1127.
78 S. Sunny, N. Vogel, C. Howell, T. L. Vu and J. Aizenberg, *Adv. Funct. Mater.*, 2014, **24**, 6658-6667.
79 H. Bazyar, S. Javadpour and R. G. H. Lammertink, *Adv. Mat. Interfaces*, 2016, **3**, 6.
80 D. Daniel, J. V. I. Timonen, R. P. Li, S. J. Velling and J. Aizenberg, *Nat. Phys.*, 2017, **13**, 1020.
81 G. K. Sirohia and X. Dai, *Int. J. Heat Mass Transfer*, 2019, **140**, 777-785.
82 P. W. Wilson, W. Lu, H. Xu, P. Kim, M. J. Kreder, J. Alvarenga and J. Aizenberg, *Phys. Chem. Chem. Phys.*, 2013, **15**, 581-585.

83 X. Dai, N. Sun, S. O. Nielsen, B. B. Stogin, J. Wang, S. Yang and T.-S. Wong, *Sci. Adv.*, 2018, **4**, eaaq0919.
84 P. S. Brown and B. Bhushan, *Sci. Rep.*, 2017, **7**, 6.
85 P. S. Brown and B. Bhushan, *J. Colloid Interface Sci.*, 2017, **487**, 437-443.
86 J. Sun and P. B. Weisensee, *Soft Matter*, 2019, **15**, 4808-4817.
87 Z. Dong, M. F. Schumann, M. J. Hokkanen, B. Chang, A. Welle, Q. Zhou, R. H. A. Ras, Z. Xu, M. Wegener and P. A. Levkin, *Adv. Mater.*, 2018, **30**, e1803890.
88 H. Geng and S. K. Cho, *Lab Chip*, 2019, **19**, 2275-2283.
89 J. C. Guo, D. H. Wang, Q. Q. Sun, L. X. Li, H. X. Zhao, D. S. Wang, J. X. Cui, L. Q. Chen and X. Deng, *Adv. Mat. Interfaces*, 2019, **6**, 1900653.
90 C. Hao, J. Li, Y. Liu, X. Zhou, Y. Liu, R. Liu, L. Che, W. Zhou, D. Sun, L. Li, L. Xu and Z. Wang, *Nat. Commun.*, 2015, **6**, 7986.
91 C. Howell, T. L. Vu, C. P. Johnson, X. Hou, O. Ahanotu, J. Alvarenga, D. C. Leslie, O. Uzun, A. Waterhouse, P. Kim, M. Super, M. Aizenberg, D. E. Ingber and J. Aizenberg, *Chem. Mater.*, 2015, **27**, 1792-1800.
92 W. Lei, J. Bruchmann, J. L. Ruping, P. A. Levkin and T. Schwartz, *Adv. Sci.*, 2019, **6**, 1900519.
93 M. M. Liu, Y. Y. Hou, J. Li, L. Tie and Z. G. Guo, *Chem. Eng. J.*, 2018, **337**, 462-470.
94 Q. Liu, Y. Yang, M. Huang, Y. X. Zhou, Y. Y. Liu and X. D. Liang, *Appl. Surf. Sci.*, 2015, **346**, 68-76.
95 K. Manabe, S. Nishizawa, K. H. Kyung and S. Shiratori, *ACS Appl. Mater. Interfaces*, 2014, **6**, 13985-13993.
96 I. Okada and S. Shiratori, *ACS Appl. Mater. Interfaces*, 2014, **6**, 1502-1508.
97 D. Paulssen, W. Feng, I. Pini and P. A. Levkin, *Adv. Mat. Interfaces*, 2018, **5**, 1800852.
98 Z. Wang and Z. Guo, *Nanoscale*, 2018, **10**, 19879-19889.
99 X. Yao, Y. Hu, A. Grinthal, T. S. Wong, L. Mahadevan and J. Aizenberg, *Nat. Mater*, 2013, **12**, 529-534.
100 M. Yu, M. Liu, Y. Hou, S. Fu, L. Zhang, M. Li and D. Wang, *J. Mater. Sci.*, 2019, **55**, 4225-4237.
101 S. Zouaghi, T. Six, S. Bellayer, S. Moradi, S. G. Hatzikiriakos, T. Dargent, V. Thomy, Y. Coffinier, C. Andre, G. Delaplace and M. Jimenez, *ACS Appl. Mater. Interfaces*, 2017, **9**, 26565-26573.
102 S. J. Lee, H. N. Kim, W. Choi, G. Y. Yoon and E. Seo, *Soft Matter*, 2019, **15**, 8459-8467.
103 Q. Li and Z. Guo, *J. Colloid Interface Sci.*, 2019, **536**, 507-515.
104 J. Guo, W. Fang, A. Welle, W. Feng, I. Filpponen, O. J. Rojas and P. A. Levkin, *ACS Appl. Mater. Interfaces*, 2016, **8**, 34115-34122.
105 D. Paulssen, S. Hardt and P. A. Levkin, *ACS Appl. Mater. Interfaces*, 2019, **11**, 16130-16138.
106 J. X. Wu, B. W. Zhang, B. J. Wang and J. Y. Li, *Chemnanomat*, 2017, **3**, 869-873.
107 A. C. Glavan, R. V. Martinez, A. B. Subramaniam, H. J. Yoon, R. M. D. Nunes, H. Lange, M. M. Thuo and G. M. Whitesides, *Adv. Funct. Mater.*, 2014, **24**, 60-70.
108 M. F. B. Sousa, H. C. Loureiro and C. A. Bertran, *Surf. Coat. Technol.*, 2020, **382**, 125160.
109 Y. Liu, Y. Tian, J. Chen, H. Gu, J. Liu, R. Wang, B. Zhang, H. Zhang and Q. Zhang, *Colloids Surf. Physicochem. Eng. Aspects*, 2020, **588**, 124384.
110 B. J. Zhang, K. J. Kim and C. Y. Lee, *Exp. Therm Fluid Sci.*, 2018, **96**, 216-223.
111 S. Anand, A. T. Paxson, R. Dhiman, J. D. Smith and K. K. Varanasi, *ACS Nano*, 2012, **6**, 10122-10129.
112 K. Rykaczewski, S. Anand, S. B. Subramanyam and K. K. Varanasi, *Langmuir*, 2013, **29**, 5230-5238.
113 K. Rykaczewski, A. T. Paxson, M. Staymates, M. L. Walker, X. Sun, S. Anand, S. Srinivasan, G. H. McKinley, J. Chinn, J. H. Scott and K. K. Varanasi, *Sci. Rep.*, 2014, **4**, 4158.
114 G. Chaniel, M. Frenkel, V. Multanen and E. Bormashenko, *Colloids Surf. Physicochem. Eng. Aspects*, 2017, **522**, 355-360.
115 A. Eifert, D. Paulssen, S. N. Varanakkottu, T. Baier and S. Hardt, *Adv. Mat. Interfaces*, 2014, **1**, 1300138.
116 C. L. Gao, L. Wang, Y. C. Lin, J. T. Li, Y. F. Liu, X. Li, S. L. Feng and Y. M. Zheng, *Adv. Funct. Mater.*, 2018, **28**, 1803072.
117 H. Liu, P. Zhang, M. Liu, S. Wang and L. Jiang, *Adv. Mater.*, 2013, **25**, 4477-4481.
118 G. Shi, Y. Wang, S. Derakhshanfar, K. Xu, W. Zhong, G. Luo, T. Liu, Y. Wang, J. Wu and M. Xing, *Mater. Sci. Eng., C*, 2019, **100**, 915-927.
119 N. Sinn, M. T. Schür and S. Hardt, *Appl. Phys. Lett.*, 2019, **114**, 213704.
120 X. Zhu, J. Lu, X. Li, B. Wang, Y. Song, X. Miao, Z. Wang and G. Ren, *Ind. Eng. Chem. Res.*, 2019, **58**, 8148-8153.
121 A. Gao, J. Liu, L. Ye, C. Schönecker, M. Kappl, H.-J. Butt and W. Steffen, *Langmuir*, 2019, **35**, 14042-14048.
122 J. H. Kim and J. P. Rothstein, *Exp. Fluids*, 2016, **57**, 9.
123 A. Al-Sharafi, B. S. Yilbas and H. Ali, *J. Heat Trans.-T ASME*, 2017, **139**, 14.
124 J. Cui, D. Daniel, A. Grinthal, K. Lin and J. Aizenberg, *Nat. Mater*, 2015, **14**, 790-795.
125 W. Q. He, P. Liu, J. K. Jiang, M. J. Liu, H. L. Li, J. Q. Zhang, Y. Luo, H. Y. Cheung and X. Yao, *J. Mater. Chem. A*, 2018, **6**, 4199-4208.
126 C. Howell, T. L. Vu, J. J. Lin, S. Kolle, N. Juthani, E. Watson, J. C. Weaver, J. Alvarenga and J. Aizenberg, *ACS Appl. Mater. Interfaces*, 2014, **6**, 13299-13307.
127 J. Jiang, J. Gao, H. Zhang, W. He, J. Zhang, D. Daniel and X. Yao, *Proc. Natl. Acad. Sci. U.S.A.*, 2019, **116**, 2482-2487.
128 A. Keiser, L. Keiser, C. Clanet and D. Quéré *Soft Matter*, 2017, **13**, 6981-6987.
129 D. P. Regan, C. Lilly, A. Weigang, L. R. White, E. J. LeClair, A. Collins and C. Howell, *Biointerphases*, 2019, **14**, 041005.
130 L. R. J. Scarratt, L. Zhu and C. Neto, *Langmuir*, 2019, **35**, 2976-2982.
131 S. Sunny, G. Cheng, D. Daniel, P. Lo, S. Ochoa, C. Howell, N. Vogel, A. Majid and J. Aizenberg, *Proc. Natl. Acad. Sci. U.S.A.*, 2016, **113**, 11676-11681.
132 M. Tonelli, S. Peppou-Chapman, F. Ridi and C. Neto, *J. Phys. Chem. C*, 2019, **123**, 2987-2995.
133 C. S. Ware, T. Smith-Palmer, S. Peppou-Chapman, L. R. J. Scarratt, E. M. Humphries, D. Balzer and C. Neto, *ACS Appl. Mater. Interfaces*, 2018, **10**, 4173-4182.
134 C. Q. Wei, G. F. Zhang, Q. H. Zhang, X. L. Zhan and F. Q. Chen, *ACS Appl. Mater. Interfaces*, 2016, **8**, 34810-34819.
135 S. Amini, S. Kolle, L. Petrone, O. Ahanotu, S. Sunny, C. N. Sutanto, S. Hoon, L. Cohen, J. C. Weaver, J. Aizenberg, N. Vogel and A. Miserez, *Science*, 2017, **357**, 668-673.
136 H. Zhao, L. O. Prieto-López, X. Zhou, X. Deng and J. Cui, *Adv. Mat. Interfaces*, 2019, **6**, 1901028.
137 Y. Zheng, J. Cheng, C. Zhou, H. Xing, X. Wen, P. Pi and S. Xu, *Langmuir*, 2017, **33**, 4172-4177.
138 J. Hui Guan, E. Ruiz-Gutierrez, B. B. Xu, D. Wood, G. McHale, R. Ledesma-Aguilar and G. G. Wells, *Soft Matter*, 2017, **13**, 3404-3410.
139 B. Jin, M. Liu, Q. Zhang, X. Zhan and F. Chen, *Langmuir*, 2017, **33**, 10340-10350.
140 J. T. Luo, N. R. Geraldi, J. H. Guan, G. McHale, G. G. Wells and Y. Q. Fu, *Phys. Rev. Appl.*, 2017, **7**, 9.
141 G. McHale, B. V. Orme, G. G. Wells and R. Ledesma-Aguilar, *Langmuir*, 2019, **35**, 4197-4204.
142 M. Sharma, P. K. Roy, R. Pant and K. Khare, *Colloids and Surfaces A: Physicochemical and Engineering Aspects*, 2019, **562**, 377-382.

143 N. R. Geraldi, J. H. Guan, L. E. Dodd, P. Maiello, B. B. Xu, D. Wood, M. I. Newton, G. G. Wells and G. McHale, *Sci. Rep.*, 2019, **9**, 13280.

144 Z. Wang, L. Heng and L. Jiang, *J. Mater. Chem. A*, 2018, **6**, 3414-3421.

145 S. J. Goodband, S. Armstrong, H. Kusumaatmaja and K. Voïtchovsky, *Langmuir*, 2020, DOI: 10.1021/acs.langmuir.0c00059.

146 P. Baumli, H. Teisala, H. Bauer, D. Garcia-Gonzalez, V. Damle, F. Geyer, M. D'Acunzi, A. Kaltbeitzel, H. J. Butt and D. Vollmer, *Adv. Sci.*, 2019, **6**, 1900019.

147 P. Juuti, J. Haapanen, C. Stenroos, H. Niemela-Anttonen, J. Harra, H. Koivuluoto, H. Teisala, J. Lahti, M. Tuominen, J. Kuusipalo, P. Vuoristo and J. M. Makela, *Appl. Phys. Lett.*, 2017, **110**, 4.

148 J. Zhang and Z. Yao, *J. Bionic Eng.*, 2019, **16**, 291-298.

149 X. Zhang, L. Sun, Y. Wang, F. Bian, Y. Wang and Y. Zhao, *Proc. Natl. Acad. Sci. U.S.A.*, 2019, **116**, 20863.

150 S. Baek and K. Yong, *Appl. Surf. Sci.*, 2020, **506**, 144689.

151 J. Cui, H. Zhu, Z. Tu, D. Niu, G. Liu, Y. Bei and Q. Zhu, *J. Mater. Sci.*, 2018, **54**, 2729-2739.

152 W. Cui and T. A. Pakkanen, *Appl. Surf. Sci.*, 2019, **504**, 144061.

153 V. G. Damle, A. Tummala, S. Chandrashekar, C. Kido, A. Roopesh, X. Sun, K. Doudrick, J. Chinn, J. R. Lee, T. P. Burgin and K. Rykaczewski, *ACS Appl. Mater. Interfaces*, 2015, **7**, 4224-4232.

154 J. Lee, J. Yoo, J. Kim, Y. Jang, K. Shin, E. Ha, S. Ryu, B. G. Kim, S. Wooh and K. Char, *ACS Appl. Mater. Interfaces*, 2019, **11**, 6550-6560.

155 R. Togasawa, F. Ohnuki and S. Shiratori, *ACS Appl. Nano Mater.*, 2018, **1**, 1758-1765.

156 Y. H. Yeong, C. Wang, K. J. Wynne and M. C. Gupta, *ACS Appl. Mater. Interfaces*, 2016, **8**, 32050-32059.

157 D. Zhang, Y. Xia, X. Chen, S. Shi and L. Lei, *Langmuir*, 2019, **35**, 8276-8284.

158 J.-H. Kim and J. P. Rothstein, *Langmuir*, 2016, **32**, 10166-10176.

159 S. Wooh and H.-J. Butt, *Angew. Chem. Int. Ed.*, 2017, **56**, 4965-4969.

160 S. Barthwal, B. Lee and S.-H. Lim, *Appl. Surf. Sci.*, 2019, **496**, 143677.

161 X. D. He, W. B. Qiang, C. Du, Q. F. Shao, X. P. Zhang and Y. Q. Deng, *J. Mater. Chem. A*, 2017, **5**, 19159-19167.

162 E. Kasapgil, I. Anac and H. Y. Erbil, *Colloids Surf. Physicochem. Eng. Aspects*, 2019, **560**, 223-232.

163 S. Ozbay, C. Yuceel and H. Y. Erbil, *ACS Appl. Mater. Interfaces*, 2015, **7**, 22067-22077.

164 R. Pant, P. K. Roy, A. K. Nagarajan and K. Khare, *RSC Adv.*, 2016, **6**, 15002-15007.

165 H. Zhang, Y. Liang, P. Wang and D. Zhang, *Prog. Org. Coat.*, 2019, **132**, 132-138.

166 P. Zhang, G. Liu, D. Zhang and H. Chen, *ACS Appl. Mater. Interfaces*, 2018, **10**, 33713-33720.

167 S. K. Ujjain, P. K. Roy, S. Kumar, S. Singha and K. Khare, *Sci. Rep.*, 2016, **6**, 35524.

168 M. Tenjimbayashi, J. Y. Park, J. Muto, Y. Kobayashi, R. Yoshikawa, Y. Monnai and S. Shiratori, *ACS Biomater. Sci. Eng.*, 2018, **4**, 1871-1879.

169 L. Rapoport, B. R. Solomon and K. K. Varanasi, *ACS Appl. Mater. Interfaces*, 2019, **11**, 16123-16129.

170 V. Multanen, G. Whyman, E. Shulzinger, V. Valtsifer and E. Bormashenko, *Colloids Surf. Physicochem. Eng. Aspects*, 2018, **538**, 133-139.

171 U. Manna and D. M. Lynn, *Adv. Mater.*, 2015, **27**, 3007-3012.

172 D. Wu, L. Ma, F. Zhang, H. Qian, B. Minhas, Y. Yang, X. Han and D. Zhang, *Mater. Des.*, 2020, **185**, 108236.

173 K. Manabe, K.-H. Kyung and S. Shiratori, *ACS Appl. Mater. Interfaces*, 2015, **7**, 4763-4771.

174 G. Zhang, Q. Zhang, T. Cheng, X. Zhan and F. Chen, *Langmuir*, 2018, **34**, 4052-4058.

175 D. Wang, Z. Guo and W. Liu, *Research*, 2019, **2019**, 1649427.

176 F. Schellenberger, J. Xie, N. Encinas, A. Hardy, M. Klapper, P. Papadopoulos, H. J. Butt and D. Vollmer, *Soft Matter*, 2015, **11**, 7617-7626.

177 X. Q. Wang, C. D. Gu, L. Y. Wang, J. L. Zhang and J. P. Tu, *Chem. Eng. J.*, 2018, **343**, 561-571.

178 Y. Galvan, K. R. Phillips, M. Haumann, P. Wasserscheid, R. Zarraga and N. Vogel, *Langmuir*, 2018, **34**, 6894-6902.

179 T. V. Charpentier, A. Neville, S. Baudin, M. J. Smith, M. Euvrard, A. Bell, C. Wang and R. Barker, *J. Colloid Interface Sci.*, 2015, **444**, 81-86.

180 M. Tress, S. Karpitschka, P. Papadopoulos, J. H. Snoeijer, D. Vollmer and H. J. Butt, *Soft Matter*, 2017, **13**, 3760-3767.

181 D. F. Miranda, C. Urata, B. Masheder, G. J. Dunderdale, M. Yagihashi and A. Hozumi, *APL Mater.*, 2014, **2**, 056108.

182 S. Anand, K. Rykaczewski, S. B. Subramanyam, D. Beysens and K. K. Varanasi, *Soft Matter*, 2015, **11**, 69-80.

183 S. Rowthu, E. E. Balic and P. Hoffmann, *Nanotechnology*, 2017, **28**, 505605.

184 V. Singh, Y. J. Sheng and H. K. Tsao, *J. Taiwan Inst. Chem. E*, 2019, **97**, 96-104.

185 M. Maszewska, A. Florowska, E. Dluzewska, M. Wroniak, K. Marciniak-Lukasiak and A. Zbikowska, *Molecules*, 2018, **23**.

186 J. X. Chen, C. Howell, C. A. Haller, M. S. Patel, P. Ayala, K. A. Moravec, E. B. Dai, L. Y. Liu, I. Sotiri, M. Aizenberg, J. Aizenberg and E. L. Chaikof, *Biomaterials*, 2017, **113**, 80-92.

187 Y. Tsuruki, M. Sakai, T. Isobe, S. Matsushita and A. Nakajima, *J. Mater. Res.*, 2014, **29**, 1546-1555.

188 Q. Wei, C. Schlaich, S. Prevost, A. Schulz, C. Bottcher, M. Gradzielski, Z. Qi, R. Haag and C. A. Schalley, *Adv. Mater.*, 2014, **26**, 7358-7364.

189 J. Yin, M. L. Mei, Q. Li, R. Xia, Z. Zhang and C. H. Chu, *Sci. Rep.*, 2016, **6**, 25924.

190 L. Xiao, J. Li, S. Mieszkin, A. Di Fino, A. S. Clare, M. E. Callow, J. A. Callow, M. Grunze, A. Rosenhahn and P. A. Levkin, *ACS Appl. Mater. Interfaces*, 2013, **5**, 10074-10080.

191 N. Wang, D. S. Xiong, S. Pan, K. Wang, Y. Shi and Y. L. Deng, *New J. Chem.*, 2017, **41**, 1846-1853.

192 I. You, T. G. Lee, Y. S. Nam and H. Lee, *ACS Nano*, 2014, **8**, 9016-9024.

193 C. C. Chen, C. J. Chen, S. A. Chen, W. H. Li and Y. M. Yang, *Colloid. Polym. Sci.*, 2018, **296**, 319-326.

194 Y. E. Liang, I. K. Maharsih, Y. J. Sheng and H. K. Tsao, *Exp. Therm Fluid Sci.*, 2019, **105**, 216-222.

195 S. Rowthu and P. Hoffmann, *ACS Appl. Mater. Interfaces*, 2018, **10**, 10560-10570.

196 K. K. Tseng, W. H. Lu, C. W. Han and Y. M. Yang, *Thin Solid Films*, 2018, **653**, 67-72.

197 P. Sartori, E. Guglielmin, D. Ferraro, D. Filippi, A. Zaltron, M. Pierno and G. Mistura, *J. Fluid Mech.*, 2019, **876**, R4.

198 J. Yang, H. Song, H. Ji and B. Chen, *J. Adhes. Sci. Technol.*, 2014, **28**, 1949-1957.

199 J. Zhang, C. Gu and J. Tu, *ACS Appl. Mater. Interfaces*, 2017, **9**, 11247-11257.

200 C. C. Chang, C. J. Wu, Y. J. Sheng and H. K. Tsao, *RSC Adv.*, 2016, **6**, 19214-19222.

201 Y. Wang, W. Zhao, W. Wu, C. Wang, X. Wu and Q. Xue, *ACS Appl. Bio. Mater.*, 2018, **2**, 155-162.

202 A. Waterhouse, D. C. Leslie, K. Lightbown, D. Antonoff, S. Lightbown, N. Dimitrakakis, J. B. Hicks-Berthet, C. N. Leslie, M. Super, D. E. Ingber and M. B. Ackerman, *ACS Biomater. Sci. Eng.*, 2018, **5**, 420-424.

203 M. Badv, C. Alonso-Cantu, A. Shakeri, Z. Hosseinidoust, J. I. Weitz and T. F. Didar, *ACS Biomater. Sci. Eng.*, 2019, **5**, 6485-6496.
204 M. Badv, S. M. Imani, J. I. Weitz and T. F. Didar, *ACS Nano*, 2018, **12**, 10890-10902.
205 Q. Ma, W. Wang and G. N. Dong, *Colloids Surf. Physicochem. Eng. Aspects*, 2019, **577**, 17-26.
206 W. Ma, Y. Higaki, H. Otsuka and A. Takahara, *Chem. Commun.*, 2013, **49**, 597-599.
207 Y. Ouyang, J. Zhao, R. Qiu, S. Hu, Y. Zhang and P. Wang, *Colloids Surf. Physicochem. Eng. Aspects*, 2018, **559**, 297-304.
208 R. Qiu, Q. Zhang, P. Wang, L. N. Jiang, J. Hou, W. M. Guo and H. X. Zhang, *Colloids Surf. Physicochem. Eng. Aspects*, 2014, **453**, 132-141.
209 P. Wang, Z. Lu and D. Zhang, *Corros. Sci.*, 2015, **93**, 159-166.
210 Y. S. Xu and M. Y. Liu, *Surf. Coat. Technol.*, 2016, **307**, 332-344.
211 D. Zhao, X. D. Xu, S. S. Yuan, S. J. Yan, X. H. Wang, S. F. Luan and J. H. Yin, *Chin. J. Polym. Sci.*, 2017, **35**, 887-896.
212 S. B. Subramanyam, K. Rykaczewski and K. K. Varanasi, *Langmuir*, 2013, **29**, 13414-13418.
213 M. J. Goudie, J. Pant and H. Handa, *Sci. Rep.*, 2017, **7**, 13.
214 M. J. Coady, M. Wood, G. Q. Wallace, K. E. Nielsen, A. M. Kietzig, F. Lagugne-Labarthet and P. J. Ragogna, *ACS Appl. Mater. Interfaces*, 2018, **10**, 2890-2896.
215 X. Jing and Z. Guo, *ACS Appl. Mater. Interfaces*, 2019, **11**, 35949-35958.
216 Y. Ouyang, J. Zhao, R. Qiu, S. Hu, M. Chen and P. Wang, *Surf. Coat. Technol.*, 2019, **367**, 148-155.
217 Y. Ouyang, J. Zhao, R. Qiu, S. Hu, H. Niu, Y. Zhang and M. Chen, *Surf. Coat. Technol.*, 2020, **381**, 125143.
218 M. Tas, H. Memon, F. Xu, I. Ahmed and X. Hou, *Colloids Surf. Physicochem. Eng. Aspects*, 2019, DOI: https://doi.org/10.1016/j.colsurfa.2019.124177, 124177.
219 J. L. Yong, F. Chen, Q. Yang, Y. Fang, J. L. Huo, J. Z. Zhang and X. Hou, *Adv. Mat. Interfaces*, 2017, **4**, 7.
220 X. Zhou, Y. Y. Lee, K. S. L. Chong and C. B. He, *J. Mater. Chem. B*, 2018, **6**, 440-448.
221 L. Zhu, J. Xue, Y. Wang, Q. Chen, J. Ding and Q. Wang, *ACS Appl. Mater. Interfaces*, 2013, **5**, 4053-4062.
222 S. Yuan, X. Zhang, D. Lin, F. Xu, Y. Li and H. Wang, *Prog. Org. Coat.*, 2020, **142**, 105563.
223 T. Kajiya, F. Schellenberger, P. Papadopoulos, D. Vollmer and H. J. Butt, *Sci. Rep.*, 2016, **6**, 23687.
224 T. S. Awad, D. Asker and B. D. Hatton, *ACS Appl. Mater. Interfaces*, 2018, **10**, 22902-22912.
225 D. Q. Wu, D. W. Zhang, Y. W. Ye, L. W. Ma, B. Minhas, B. Liu, H. A. Terryn, J. M. C. Mol and X. G. Li, *Chem. Eng. J.*, 2019, **368**, 138-147.
226 D. Wu, L. Ma, B. Liu, D. Zhang, B. Minhas, H. Qian, H. A. Terryn and J. M. C. Mol, *J. Mater. Sci. Technol.*, 2020, DOI: 10.1016/j.jmst.2019.12.008.
227 T. Yamazaki, M. Tenjimbayashi, K. Manabe, T. Moriya, H. Nakamura, T. Nakamura, T. Matsubayashi, Y. Tsuge and S. Shiratori, *Ind. Eng. Chem. Res.*, 2019, **58**, 2225-2234.
228 P. Irajizad, M. Hasnain, N. Farokhnia, S. M. Sajadi and H. Ghasemi, *Nat. Commun.*, 2016, **7**, 13395.
229 A. Ahmed, I. Hassan, I. M. Mosa, E. Elsanadidy, M. Sharafeldin, J. F. Rusling and S. Ren, *Adv. Mater.*, 2019, **31**, 1807201.
230 K. S. Khalil, S. R. Mahmoudi, N. Abu-dheir and K. K. Varanasi, *Appl. Phys. Lett.*, 2014, **105**, 041604.
231 W. Wang, J. V. I. Timonen, A. Carlson, D.-M. Drotlef, C. T. Zhang, S. Kolle, A. Grinthal, T.-S. Wong, B. Hatton, S. H. Kang, S. Kennedy, J. Chi, R. T. Blough, M. Sitti, L. Mahadevan and J. Aizenberg, *Nature*, 2018, **559**, 77-82.
232 X. Yao, J. Ju, S. Yang, J. Wang and L. Jiang, *Adv. Mater.*, 2014, **26**, 1895-1900.
233 B. L. Wang, L. Heng and L. Jiang, *ACS Appl. Mater. Interfaces*, 2018, **10**, 7442-7450.
234 A. M. Pornea, J. M. C. Puguan, V. G. Deonikar and H. Kim, *J. Ind. Eng. Chem.*, 2019, **82**, 211-219.
235 C. Chen, L. Zhou, L.-A. Shi, S. Zhu, Z. Huang, C. Xue, J. Li, Y. Hu, D. Wu and J. Chu, *ACS Appl. Mater. Interfaces*, 2019, **12**, 1895-1904.
236 Y. Zhuo, F. Wang, S. Xiao, J. He and Z. Zhang, *ACS Omega*, 2018, **3**, 10139-10144.
237 P. Guo, Y. Sun, Y. Zhang, X. Hou, Y. Song and J.-J. Wang, *ChemPhysChem*, 2019, **20**, 946-952.
238 K. Manabe, T. Matsubayashi, M. Tenjimbayashi, T. Moriya, Y. Tsuge, K.-H. Kyung and S. Shiratori, *ACS Nano*, 2016, **10**, 9387-9396.
239 D. O'Hagan, *Chem. Soc. Rev.*, 2008, **37**, 308-319.
240 F. Weinhold and R. West, *Organometallics*, 2011, **30**, 5815-5824.
241 M. J. Owen and P. R. Dvornic, in *Silicone Surface Science*, Springer, 2012, DOI: 10.1007/978-94-007-3876-8, ch. 1, pp. 1-21.
242 S. Karpitschka, S. Das, M. van Gorcum, H. Perrin, B. Andreotti and J. H. Snoeijer, *Nat. Commun.*, 2015, **6**, 7891.
243 L. Guo, G. H. Tang and S. Kumar, *Langmuir*, 2019, **35**, 16377-16387.
244 S. Sett, X. Yan, G. Barac, L. W. Bolton and N. Miljkovic, *ACS Appl. Mater. Interfaces*, 2017, **9**, 36400-36408.
245 D. J. Preston, Y. Song, Z. Lu, D. S. Antao and E. N. Wang, *ACS Appl. Mater. Interfaces*, 2017, **9**, 42383-42392.
246 C. J. van Oss, *Interfacial Forces in Aqueous Media*, 2006.
247 A. Carlson, P. Kim, G. Amberg and H. A. Stone, *Europhys. Lett.*, 2013, **104**, 34008.
248 J. Isrealachvili, *Intermolecular & Surface Forces*, Elsevier, 2nd edn., 1991.
249 M. J. Kratochvil, M. A. Welsh, U. Manna, B. J. Ortiz, H. E. Blackwell and D. M. Lynn, *ACS Infec. Dis.*, 2016, **2**, 509-517.
250 U. Manna, N. Raman, M. A. Welsh, Y. M. Zayas-Gonzalez, H. E. Blackwell, S. P. Palecek and D. M. Lynn, *Adv. Funct. Mater.*, 2016, **26**, 3599-3611.
251 Z. F. Gao, R. Liu, J. Wang, J. Dai, W.-H. Huang, M. Liu, S. Wang, F. Xia and L. Jiang, *Chem*, 2018, **4**, 2929-2943.
252 J. Wang, Y. Huang, K. You, X. Yang, Y. Song, H. Zhu, F. Xia and L. Jiang, *ACS Appl. Mater. Interfaces*, 2019, **11**, 7591-7599.
253 H. Xiao and S. Liu, *Mater. Des.*, 2017, **135**, 319-332.
254 L. Liu, M. Zhou, L. Jin, L. Li, Y. Mo, G. Su, X. Li, H. Zhu and Y. Tian, *Friction*, 2019, **7**, 199-216.
255 Z. Chen, X. Liu, Y. Liu, S. Gunsel and J. Luo, *Sci. Rep.*, 2015, **5**, 12869.
256 C. Corti and P. Savelli, *Journal of Synthetic Lubrication*, 1993, **9**, 311-330.
257 SLIPS Foul Protect Bottom Paints From AST, https://slipsfoulprotect.com/, (accessed 10/24/2019, 2019).
258 R. R. Brooks, *Great Britian Pat.,* EP0329375A1, 1989.
259 D. P. Edwards, T. G. Nevell, B. A. Plunkett and B. C. Ochiltree, *Int. Biodeterior. Biodegrad.*, 1994, **34**, 349-359.
260 T. G. Nevell, D. P. Edwards, A. J. Davis and R. A. Pullin, *Biofouling*, 1996, **10**, 199-212.
261 J. Stein, K. Truby, C. Darkangelo Wood, J. Stein, M. Gardner, G. Swain, C. Kavanagh, B. Kovach, M. Schultz, D. Wiebe, E. Holm, J. Montemarano, D. Wendt, C. Smith and A. Meyer, *Biofouling*, 2003, **19**, 71-82.
262 M. Nendza, *Mar. Pollut. Bull.*, 2007, **54**, 1190-1196.
263 C. Stevens, D. E. Powell, P. Makela and C. Karman, *Mar. Pollut. Bull.*, 2001, **42**, 536-543.
264 N. J. Fendinger, in *Organosilicon Chemistry Set*, 2005, DOI: doi:10.1002/9783527620777.ch103c, pp. 626-638.

265 W. A. Bruggeman, D. Weber-Fung, A. Opperhuizen, J. VanDerSteen, A. Wijbenga and O. Hutzinger, *Toxicol. Environ, Chem.*, 1984, **7**, 287-296.

266 R. B. Annelin and C. L. Frye, *Sci. Total Environ.*, 1989, **83**, 1-11.

267 L. D. Chambers, K. R. Stokes, F. C. Walsh and R. J. K. Wood, *Surf. Coat. Technol.*, 2006, **201**, 3642-3652.

268 A. J. Martin-Rodriguez, J. M. F. Babarro, F. Lahoz, M. Sanson, V. S. Martin, M. Norte and J. J. Fernandez, *Plos One*, 2015, **10**, 30.

269 M. A. K. Khalil, R. A. Rasmussen, J. A. Culbertson, J. M. Prins, E. P. Grimsrud and M. J. Shearer, *Environ. Sci. Technol.*, 2003, **37**, 4358-4361.

270 S. Rao and K. Riahi, *Energy J.*, 2006, **SI2006**, 177-200.

271 C. J. Young, M. D. Hurley, T. J. Wallington and S. A. Mabury, *Environ. Sci. Technol.*, 2006, **40**, 2242-2246.

272 K. P. Shine, L. K. Gohar, M. D. Hurley, G. Marston, D. Martin, P. G. Simmonds, T. J. Wallington and M. Watkins, *Atmos. Environ.*, 2005, **39**, 1759-1763.

273 T. B. Watson, R. Wilke, R. N. Dietz, J. Heiser and P. Kalb, *Environ. Sci. Technol.*, 2007, **41**, 6909-6913.

274 S. Mizael, Shiny, strong hair without silicone oils, https://www.cossma.com/ingredients/article/shiny-strong-hair-without-silicone-oils-35227.html, (accessed 05/11/2019, 2019).

275 D. Mackay, C. E. Cowan-Ellsberry, D. E. Powell, K. B. Woodburn, S. Xu, G. E. Kozerski and J. Kim, *Environ. Toxicol. Chem.*, 2015, **34**, 2689-2702.

276 A. Theimann, J. Scholze and M. Salmina-Peterson, *Journal*, 2015, **4**, 12-15.

277 C. Consalvo, S. Panebianco, B. Pignataro, G. Compagnini and O. Puglisi, *J. Phys. Chem. B*, 1999, **103**, 4687-4692.

278 B. Pignataro, C. Consalvo, G. Compagnini and A. Licciardello, *Chem. Phys. Lett.*, 1999, **299**, 430-436.

279 F. Caravieri, Nature-inspired concepts for hair needs, https://www.cossma.com/ingredients/article/nature-inspired-concepts-for-hair-needs-35702.html, (accessed 05/11/2019, 2019).

280 R. Gusain and O. P. Khatri, *RSC Adv.*, 2016, **6**, 3462-3469.

281 R. Goto, R. Kado, K. Muramoto and H. Kamiya, *Biofouling*, 1992, **6**, 61-68.

282 L. Sarubbo, M. d. g. Silva, D. Almeida, R. Silva, F. Almeida, H. Meira, M. Banja, A. Silva and V. Santos, *Chem. Eng. Trans.*, 2018, **64**, 655-660.

283 K. A. Soni, P. Jesudhasan, M. Cepeda, K. Widmer, G. K. Jayaprakasha, B. S. Patil, M. E. Hume and S. D. Pillai, *J. Food Prot.*, 2008, **71**, 134-138.

284 C. I. Castro and J. C. Briceno, *Artif. Organs*, 2010, **34**, 622-634.

285 I. Usach, R. Martinez, T. Festini and J.-E. Peris, *Adv. Ther.*, 2019, **36**, 2986-2996.

286 S. Crafoord, J. Larsson, L.-J. Hansson, J.-O. Carlsson and S. Stenkula, *Acta Ophthalmol. Scand.*, 1995, **73**, 442-445.

287 Q. Yu, K. Liu, L. Su, X. Xia and X. Xu, *Biomed Res. Int.*, 2014, **2014**, 250323.

288 F. Bottoni, M. Sborgia, P. Arpa, N. De Casa, E. Bertazzi, M. Monticelli and V. De Molfetta, *Graefes. Arch. Clin. Exp. Ophthalmol.*, 1993, **231**, 619-628.

289 H. Heimann, T. Stappler and D. Wong, *Eye (Lond)*, 2008, **22**, 1342-1359.

290 P. J. Kertes, H. Wafapoor, G. A. Peyman, N. Calixto, H. Thompson, G. A. Peyman, G. A. Williams, J. C. Werner, R. J. Olk, H. W. Flynn, H. Mani, R. Paylor, P. Campochiaro, T. O. Bennett, J. A. Schulman, K. J. Blinder, R. Wendel, R. Medlock, B. M. Glaser, J. G. Randall, C. J. Chen, J. L. Federman, W. Tasman, N. J. Mehta, N. Z. Zakov, G. E. Sanborn, N. Brourman and M. J. Elman, *Ophthalmology*, 1997, **104**, 1159-1165.

291 K. C. Lowe, *J. Fluorine Chem.*, 2001, **109**, 59-65.

292 S. F. Flaim, *Artif. Cells Blood Substit. Biotechnol.*, 1994, **22**, 1043-1054.

293 H. W. Kim and A. G. Greenburg, *Artif. Organs*, 2004, **28**, 813-828.

294 L. J. E. Jäger and J. Lutz, in *Oxygen Transport to Tissue XV*, eds. P. Vaupel, R. Zander and D. F. Bruley, Springer US, Boston, MA, 1994, DOI: 10.1007/978-1-4615-2468-7_29, pp. 221-226.

295 G. M. Vercellotti, D. E. Hammerschmidt, P. R. Craddock and H. S. Jacob, *Blood*, 1982, **59**, 1299-1304.

296 A. M. Gosselin and G. P. Biro, *Adv. Exp. Med. Biol.*, 1990, **277**, 291-299.

297 N. Jiao, G. V. Barnett, T. R. Christian, L. O. Narhi, N. H. Joh, M. K. Joubert and S. Cao, *J. Pharm. Sci.*, 2020, **109**, 640-645.

298 E. K. Purdy-Payne, J. Green, S. Zenoni, A. N. Evans and T. R. Bilski, *Surg. Infect.*, 2015, **16**, 473-477.

299 M. E. Park, A. T. Curreri, G. A. Taylor and K. Burris, *J. Clin. Aesthet. Detmatol.*, 2016, **9**, 48-51.

300 FDA Warns Against Use of Injectable Silicone for Body Contouring and Enhancement: FDA Safety Communication, https://www.fda.gov/medical-devices/safety-communications/fda-warns-against-use-injectable-silicone-body-contouring-and-enhancement-fda-safety-communication, (accessed 16/01/2020, 2020).

301 N. MacCallum, C. Howell, P. Kim, D. Sun, R. Friedlander, J. Ranisau, O. Ahanotu, J. J. Lin, A. Vena, B. Hatton, T. S. Wong and J. Aizenberg, *ACS Biomater. Sci. Eng.*, 2015, **1**, 43-51.

302 B. R. Solomon, K. S. Khalil and K. K. Varanasi, *Langmuir*, 2014, **30**, 10970-10976.

303 P. Wang, D. Zhang, S. M. Sun, T. P. Li and Y. Sun, *ACS Appl. Mater. Interfaces*, 2017, **9**, 972-982.

304 S. Yuan, Z. Li, L. Song, H. Shi, S. Luan and J. Yin, *ACS Appl. Mater. Interfaces*, 2016, **8**, 21214-21220.

305 A. K. Epstein, T. S. Wong, R. A. Belisle, E. M. Boggs and J. Aizenberg, *Proc. Natl. Acad. Sci. U.S.A.*, 2012, **109**, 13182-13187.

306 L. R. J. Scarratt, U. Steiner and C. Neto, *Adv. Colloid Interface Sci.*, 2017, **246**, 133-152.

307 F. Vüllers, S. Peppou-Chapman, M. N. Kavalenka, H. Hölscher and C. Neto, *Phys. Fluids*, 2019, **31**, 012102.

308 J. S. Li, T. Kleintschek, A. Rieder, Y. Cheng, T. Baumbach, U. Obst, T. Schwartz and P. A. Levkin, *ACS Appl. Mater. Interfaces*, 2013, **5**, 6704-6711.

309 L. R. J. Scarratt, L. Zhu and C. Neto, *Under Review*, 2020.

310 S. Armstrong, G. McHale, R. Ledesma-Aguilar and G. G. Wells, *Langmuir*, 2019, **35**, 2989-2996.

311 R. Lhermerout and K. Davitt, *Colloids Surf. Physicochem. Eng. Aspects*, 2019, **566**, 148-155.

312 Q. Wu, C. Yang, C. Su, L. Zhong, L. Zhou, T. Hang, H. Lin, W. Chen, L. Li and X. Xie, *ACS Biomater. Sci. Eng.*, 2019, **6**, 358-366.

313 C. Wei, G. Zhang, Q. Zhang, X. Zhan and F. Chen, *ACS Appl. Mater. Interfaces*, 2016, **8**, 34810-34819.

314 N. Kacker, S. K. Kumar and D. L. Allara, *Langmuir*, 1997, **13**, 6366-6369.

315 J. S. Wexler, I. Jacobi and H. A. Stone, *Phys. Rev. Lett.*, 2015, **114**, 168301.

316 E. S. Asmolov, T. V. Nizkaya and O. I. Vinogradova, *Phys. Rev. E*, 2018, **98**, 033103.

317 B. J. Rosenberg, T. Van Buren, M. K. Fu and A. J. Smits, *Phys. Fluids*, 2016, **28**, 015103.

318 T. Van Buren and A. J. Smits, *J. Fluid Mech.*, 2017, **827**, 448-456.

319 I. Jacobi, J. S. Wexler and H. A. Stone, *Phys. Fluids*, 2015, **27**, 082101.

320 J. S. Wexler, A. Grosskopf, M. Chow, Y. Fan, I. Jacobi and H. A. Stone, *Soft Matter*, 2015, **11**, 5023-5029.

321 Y. Liu, J. S. Wexler, C. Schonecker and H. A. Stone, *Phys. Rev. Fluids*, 2016, **1**, 074003.
322 C. E. Colosqui, J. S. Wexler, Y. Liu and H. A. Stone, *Physical Review Fluids*, 2016, **1**, 064101.
323 A. Mohammadi and A. J. Smits, *J. Fluid Mech.*, 2017, **826**, 128-157.
324 C. Vega, S. Peppou-Chapman and C. Neto, *Manuscript in Preparation*, 2020.
325 E. S. Asmolov, T. V. Nizkaya and O. I. Vinogradova, *arXiv preprint arXiv:2001.02972*, 2020.
326 N. Gao, F. Geyer, D. W. Pilat, S. Wooh, D. Vollmer, H.-J. Butt and R. Berger, *Nat. Phys.*, 2018, **14**, 191-196.
327 Y. Kovalenko, I. Sotiri, J. V. I. Timonen, J. C. Overton, G. Holmes, J. Aizenberg and C. Howell, *Adv. Healthc. Mater.*, 2017, **6**, 1600948.
328 H. Teisala, C. Schonecker, A. Kaltbeitzel, W. Steffen, H. J. Butt and D. Vollmer, *Phys. Rev. Fluids*, 2018, **3**, 084002.
329 H. Bazyar, P. Lv, J. A. Wood, S. Porada, D. Lohse and R. G. H. Lammertink, *Soft Matter*, 2018, **14**, 1780-1788.
330 T. Kajiya, S. Wooh, Y. Lee, K. Char, D. Vollmer and H. J. Butt, *Soft Matter*, 2016, **12**, 9377-9382.
331 J. Bian, X. X. Fu, J. Hu, Y. S. Cui, Z. W. Li, C. S. Yuan, H. X. Ge, W. D. Li and Y. F. Chen, *RSC Adv.*, 2014, **4**, 22155-22161.
332 X. Dai, B. B. Stogin, S. Yang and T.-S. Wong, *ACS Nano*, 2015, **9**, 9260-9267.
333 N. Keller, J. Bruchmann, T. Sollich, C. Richter, R. Thelen, F. Kotz, T. Schwartz, D. Helmer and B. E. Rapp, *ACS Appl. Mater. Interfaces*, 2019, **11**, 4480-4487.
334 D. Daniel, J. V. I. Timonen, R. Li, S. J. Velling, M. J. Kreder, A. Tetreault and J. Aizenberg, *Phys. Rev. Lett.*, 2018, **120**, 244503.
335 R. H. Webb, *Rep. Prog. Phys.*, 1996, **59**, 427-471.
336 G. Cox and C. J. Sheppard, *Microsc. Res. Tech.*, 2004, **63**, 18-22.
337 J. de Ruiter, F. Mugele and D. van den Ende, *Phys. Fluids*, 2015, **27**, 012104.
338 M. P. Rossi, H. H. Ye, Y. Gogotsi, S. Babu, P. Ndungu and J. C. Bradley, *Nano Lett.*, 2004, **4**, 989-993.
339 C. Semprebon, G. McHale and H. Kusumaatmaja, *Soft Matter*, 2017, **13**, 101-110.
340 M. S. Sadullah, C. Semprebon and H. Kusumaatmaja, *Langmuir*, 2018, **34**, 8112-8118.
341 L. Keiser, A. Keiser, M. L'Estimé, J. Bico and É. Reyssat, *Phys. Rev. Lett.*, 2019, **122**, 074501.
342 A. Keiser, P. Baumli, D. Vollmer and D. Quéré, *Phys. Rev. Fluids*, 2020, **5**, 014005.
343 N. Bjelobrk, H.-L. Girard, S. Bengaluru Subramanyam, H.-M. Kwon, D. Quéré and K. K. Varanasi, *Phys. Rev. Fluids*, 2016, **1**, 063902.
344 J. B. Boreyko, G. Polizos, P. G. Datskos, S. A. Sarles and C. P. Collier, *Proc. Natl. Acad. Sci. U.S.A.*, 2014, **111**, 7588.
345 C. Clanet, C. BÉGuin, D. Richard and D. QuÉRÉ, *J. Fluid Mech.*, 2004, **517**, 199-208.
346 F. Yeganehdoust, R. Attarzadeh, I. Karimfazli and A. Dolatabadi, *Int. J. Multiphase Flow*, 2019, **124**, 103175.